Contents

Notation

x, X	Scalar variable or function (italics)
$\boldsymbol{x}$	Vector (lowercase, bold)
x_i	Vector element
$\boldsymbol{X}$	Matrix (uppercase, bold)
$X_{i,j}$	Matrix element
$\boldsymbol{x}^T, \boldsymbol{X}^T$	Vector or matrix transpose
$\boldsymbol{x}^*$	Complex conjugate
$\boldsymbol{X}_\odot = \boldsymbol{X} \odot I$	Bialternate product of matrix
$\boldsymbol{X}^\perp$	Orthogonal complement of the subspace of $\boldsymbol{X}$
$\hat{\boldsymbol{X}}$	Estimate of $\boldsymbol{X}$
$\boldsymbol{X}_\omega$	Partial derivative, $\frac{\partial \boldsymbol{x}}{\partial \omega}$
$\lvert x \rvert$	Absolute value
$\det \boldsymbol{x}$	Determinant of $\boldsymbol{x}$
$\lVert \boldsymbol{x} \rVert_2$	Euclidean norm of x (ie. the length)
$\boldsymbol{X}^+$	Moore-Penrose pseudoinverse of $\boldsymbol{X}$
$\dot{x}, \ddot{x}$	Time derivatives
$x_{[i]}^{[i]}$	i'th iterate
$\mathcal{O}$	Order of magnitude
∇, ∇^2	Gradient/Laplacian operator
$\equiv$	Assigning equality
$j = 1, n$	$j = 1, 2, ..., n$

[title=Abbreviation,type=acronym]

Chapter 1

Introduction

In all structures, nonlinearities which will affect the dynamic behavior of the structure are present to some extend. Depending on excitation level, the structure will exhibit linear or nonlinear dynamics. Nonlinearities have always existed, but are often neglected.

To get a further understanding of the nonlinear effects present, an efficient set of tools for identification, characterization and estimation of nonlinearities in engineering structures from experimental observations is be useful.

The motivation for this thesis is to provide that understanding, hopefully giving the reader a "toolbox" applicable to nonlinear systems. A toolbox is to be understood as a collection of methods, applicable to nonlinear problems. Like modal testing is one method in the linear toolbox.

To exemplify and test this toolbox, a part of the thesis is dedicated to developing, implementing and exemplifying the methods of the toolbox numerically.

By using such a "numerical toolbox", further understanding of the nonlinear dynamics can be obtained by simulation, then what is gained by pure experiment, and hopefully assist in virtual prototyping.

One requirement for the toolbox is that it works on experimental data, e.g. time series, alone. Methods exists which can do identification and estimation, but they often require either that the Equations of Motions(EOM) are assembled or a detailed Finite Element Model(FEM) is constructed, and are thus often difficult and time consuming to use.

Another aspect of the toolbox is to quantify the size, or importance, of nonlinearity:

Even if the area of nonlinear identification and modeling have received a great deal more attention within the last ten years, it is still far behind the linear counterpart, both in theory and application. Thus a nonlinear toolbox certainly requires some specialization to use. If the nonlinearity is weak it might suffice with linear analysis, giving access to all the traditional methods, with reduced time spend on the analysis as a consequence.

Why nonlinear modeling

For nonlinear systems, the superposition and thus invariance of modes and uniqueness of solutions (e.g. the forced steady state response is dependent on the initial transient

behavior) does no longer hold, and many of the techniques from linear analysis cannot be used.

Linear system is an exception. If excited hard enough, all system displays some nonlinear behavior. But often the nonlinearity stems from joints (damping), contact (stiffness) or geometrical nonlinearities, which is why most of the literature today treats localized nonlinearity, assuming the location of the nonlinearity is known. Another reason for dealing with localized nonlinearities, is that no robust method for localization exists. In his thesis Kragh [17] test different methods for localizing nonlinearity and concludes that "it was not possible to obtain consistent localization of the nonlinearities" even for simple structures.

With the introduction of ever lighter structures, exotic materials, high speed machinery, etc., nonlinear tools are needed to fully understand the dynamics. Also to determine if nonlinear analysis is indeed needed, since this kind of analysis requires substantial more effort than linear analysis would do.

For a general introduction to nonlinear dynamics, the textbook Juel Thomsen [14] can be recommended.

Nonlinear system identification?

Kerschen et al. [16] proposed to regard the identification of nonlinear structural models as a progression through three steps: *d*etection, *c*haracterization and *e*stimation, as outlined in figure 1.0.1

The first book on the topic was Worden and Tomlinson [35], and even though many new methods has been introduced since then, it still gives a good and well written introduction to the subject as well as a overview of the common types of nonlinearity.

A comprehensive review of the development in nonlinear system identification was given by [16] and just recently in Noël and Kerschen [25]. For comparison of the many techniques in use, the reader is refereed to these reviews. In this thesis, the choice of technique will be motivated but alternative techniques will not necessarily be mentioned.

Detection

Of the three steps, detection is the easiest. During test, the structure should be excited by a sine-sweep and a mere visual inspection of the time series will show if nonlinearity is present. Signs includes skewness of the envelope, discontinuity, jumps and lack of invariance with increasing force level. The excitation level needs to be at an amplitude where the nonlinearity is activated.

Random excitation is in general not useful, as the randomness of the amplitude and phase of the excitation creates "linearized" frequency response functions (FRFs). At least multiple test with different rms levels are required, and still then it might be difficult to excite the nonlinearities, since the total power of the input spectrum is spread over the band-limited frequency range used.

The use of impact excitation, as often used in linear analysis, suffers from the same problems as random excitation. That is, the input is a broad spectrum and the energy associated with each frequency is low.

Formal methods for detection includes

1. Detection: *I*s there?
   Ascertain if nonlinearity exist in the structural behavior, e.g. yes or no.
2. Characterisation: *W*here, what and how?
   - Localize the nonlinearity, e.g. at the joint
   - Determine the type of nonlinearity e.g. Coulomb friction
     More general: is it stiffness or damping nonlinearity or both. In the case of stiffness: is it hardening or softening
   - Select the functional form of the nonlinearity, e.g. $f(x, \dot{x}) = c\,\text{sign}(\dot{y})$
3. Parameter estimation: *H*ow much?
   Calculate the coefficients of the nonlinearity model, e.g. $c = 5.47$.
   (Ideally the uncertainty should be quantified, e.g. in a probabilistic sense, $c \sim N(5.47, 1)$. But that is a very difficult task and not within the scope of this thesis)

Figure 1.0.1: *Identification process for nonlinear structural models*

- Homogeneity check
  Comparing the response of two sweeps with different forcing and calculating the cross correlation. It is a test of superposition, by testing if the two FRFs normalized with forcing overlay as they will for linear systems.

- (ordinary) Coherence function
  The coherence function compares power spectral densities (PSDs) and are required to be unity for all accessible frequencies for the system to be linear *a*nd free of noise. The advantage is that only one test is needed, but the method does not distinguish between cases of noise and nonlinearity. Instead it is recommend do use:

- Hilbert transforms
  This method detects nonlinearity by doing a Hilbert transform of the FRF, which is invariant for a linear FRF. A Hilbert transform also only requires one data set and is more sensitive to nonlinearity than the coherence function, but still reasonable easy to implement. Kragh [17] shows that the homogeneity check is superior to the Hilbert transforms, having higher sensitivity to nonlinearity.

For all of these methods it is a requirement that the nonlinearities are activated, e.g. the forcing level end frequency interval should be chosen adequately. Also, the methods are better at detecting nonlinear stiffness than nonlinear damping. This is due to the fact that the resonance peak is not shifted as with the stiffness nonlinearity case. Since the FRF is not shifted but only lowered, the cross correlation coefficient will not decrease as much as in the stiffness nonlinearity case. In general damping nonlinearity is difficult to identify and will only be touched briefly in this thesis.

Characterisation

The second step is the most important and also the most difficult, when localization is not considered. This step seeks to identify the aspects of the motion that drives the nonlinearity, e.g. displacement or velocity and a representative functional form to represent the nonlinearity.

The most used technique is the *r*estoring force surface (RFS). The RFS provides information of restoring force in the excited range. To visualize the functional of the restoring force and the dissipative force, two slices in the RFS is made: at zero displacement and zero velocity. The functional form is then found by simple inspection of the slices or fitting polynomials and perform goodness of fit.

Another characterisation method, the Morlet wavelet transform, is used to visualise how the frequency content changes with amplitude, a consequence of the energy-frequency dependency for nonlinear vibrations. The visualised instantaneous spectrum can both be used for detection of nonlinearity and help estimating the type of nonlinearity,

Estimation

The RFS method can be used for estimation as well, fitting the functional form to the surface. But in order to scale the RFS correct, an estimate of the mass (or inertia) is needed or the full EOM has to be assembled. This is often difficult for MDOF systems and violates the ambition for the toolbox: that it works on time series exclusively.

A newer method, introduced by Noel and Kerschen [24], is the frequency-domain nonlinear subspace identification(FNSI). This method works on time series alone and is able to estimate nonlinear parameters and the underlaying linear transfer function.

Beyond nonlinear system identification

When the identification steps is completed, a structural model can be build from a FEM of the underlying linear structure with the identified nonlinearities incorporated. It shall be thought of as (larger) chunks of linear sections connected through nonlinear elements. To reduce the computational time, the linear model is often reduced using the Craig-Bampton reduction technique [2].

If the predictions from the nonlinear FEM can be verified by the experimental results, the numerical model can be used to *g*et further understanding of the nonlinear dynamics. The latter is the whole goal of the identification, as it allows for uncovering new nonlinear regimes of motion and to make design modifications. The concept of using numerical experiments to assist with the design is referred to as *v*irtual prototyping.

Internal resonance

Nonlinear resonances are investigated using an extension of linear normal modes (LNMs) to nonlinear theory, the nonlinear normal modes (NNMs) described in section **??**. Where a LNM is interpreted as the deformation along the axis of the vibrating structure or the rotation, a NNM does not have such a clear interpretation. An NNM is

said to be a periodic oscillation of the underlaying undamped and unforced nonlinear system and depends on the frequency and energy of the system. Additionally, the backbone of NNMs plotted in a frequency-energy plot (FEP), track the lotus of the nonlinear frequency response curve (NFRC) for the system. Thus knowing the FEP, the resonant response at an arbitrary forcing level can be found.

Bifurcation

Using the HB method, nonlinear forced response curves(NFRCs) for a periodic excitation are calculated. The transition from a stable periodic solution to an unstable solution occurs through bifurcations. The type of bifurcation is used to qualify the type of unstable solution emerging, following the outline in [5].

Thesis outline

Section 2 introduces the theoretical methods used: NNMs, RFS and FNSI,

Section 3 introduces the numerical methods: FEM discretization and model reduction, Newmark time integration, harmonic balance and continuation for calculating NNMs and NFRF.

It also briefly discusses methods for integrating and differentiating time signals and filtering techniques.

Section 4 introduce identification and simulation of benchmark data from a nonlinear system, the COST beam, [12], which have a cubic stiffening nonlinear due to geometry and a squared nonlinearity due to clamping.

Section 5 introduces numerical experiments to investigate how the methods performs and their sensitivity to noise.

Finally section 6 contains an discussion and conclusion and suggest further studies and implementations.

1.1 Numerical example

To illustrate the methods presented, the 2-DOF system shown in figure 1.1.1 is used throughout the thesis. It will be referred to as the coupled duffing system, with parameters listed in table 1.1.1 and natural frequencies and damping ratio for the two modes listed in table 1.1.2. The equations of motion are

$$\begin{aligned} m_1\ddot{x}_1 + c\dot{x}_1 + kx_1 + \mu_1 x_1^3 + d(x_1 - x_2) &= p \\ m_2\ddot{x}_2 + c\dot{x}_2 + kx_2 + \mu_2 x_2^3 + d(x_2 - x_1) &= 0 \end{aligned} \tag{1.1.1}$$

where x_1, x_2, p all depends on time.

An example on how a real beam with different nonlinear boundary conditions is transformed into a coupled MDOF nonlinear duffing oscillator is given in Hermansen [13]

m_1 (kg)	m_2 (kg)	k (N/m)	d (N/m)	c (N/ms)	μ (N/m^3)
1	1	1	5	0.1	1

Table 1.1.1: *Linear and nonlinear parameters for the coupled Duffing system*

Mode	Frequency (rad/s)	Damping ratio (%)
1	1.00	5.00
2	3.32	1.51

Table 1.1.2: *Linear natural frequencies and damping ratios for the coupled Duffing system*

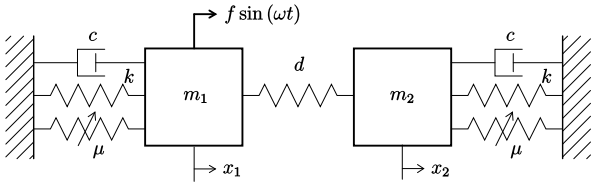

Figure 1.1.1: *Schematic representation of the coupled duffing system*

For generating data for detection and characterisation with MW and RFS, the system is simulated using a logarithmic sine sweep. For identification, a single band-limited (0-80 rad/s) normally distributed random signal with 5000 points repeated 9 times and a root mean square(rms) value of 3N is used. This signal is called a multisine. The frequencies are chosen to include the third harmonics.

Chapter 2

Methods for dection, characterization and estimation

This chapter deals with the identification process as depicted in figure 1.0.1, treating localised nonlinearities.

2.1 Wavelet transform

Due to the frequency-energy dependence of nonlinear vibrations, giving time varying frequencies for sine sweeps, the Fourier transform(FT), eq. (2.1.1) does not give useful results. To allow for a varying frequency the Short Time Fourier transform(STFT) can be used, eq. (2.1.2). Here the function to be transformed is multiplied by a window function $w(t-\tau)$ which is nonzero only for a short period of time. Practically this correspond to dividing the original signal into shorter segments of equal length and then calculate the FT of each segments, giving a 2D representation of the time-varying spectrum.

Often one want a window observation window that changes with frequency. A short window gives good time resolution, allowing for identification of when frequency content changes but poor frequency resolution. On the other hand a long window allows the frequencies to be identified but gives poor time resolution. One such window that gives a varying length is the Gaussian window function. Used with STFT, the transfer is called a Morlet wavelet(MW), eq. (2.1.3)

$$X(\omega) = \int_{-\infty}^{\infty} x(t)e^{-i\omega t}\,\mathrm{d}t \tag{2.1.1}$$

$$X(\omega,\tau) = \int_{-\infty}^{\infty} x(t)w(t-\tau)e^{-i\omega t}\,\mathrm{d}t \tag{2.1.2}$$

$$X(a,b) = \frac{1}{\sqrt{a}}\int_{-\infty}^{\infty} x(t)\psi\left(\frac{t-b}{a}\right)\mathrm{d}t \tag{2.1.3}$$

For the Morlet wavelet the window function is a Gaussian windowed complex sinusoidal, $\psi(t) = e^{-t^2/2}e^{i\omega t}$. a defines the frequency resolution by expanding/contracting the window, see figure 2.1.1 and, b is the location of the observation window in the time domain.

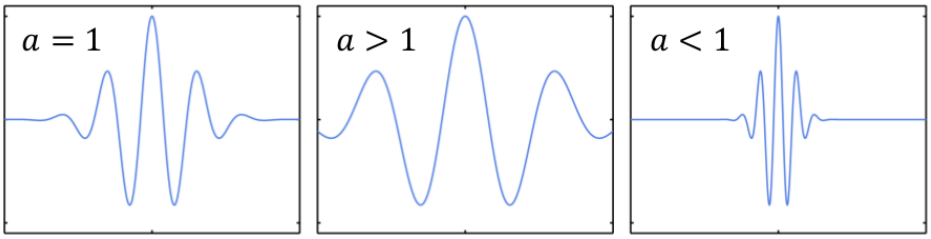

Figure 2.1.1: *Influence of a on the window length. Copied from slides given at ULG in Liege, Belgium*

Example

Figure **??**(a) shows the wavelet transform of the coupled duffing system. Fig **??**(b) shows the linear transform for comparison and fig **??**(c) the sweep. For the linear system, the two fundamental frequencies ω_1 and ω_2 along with the excitation frequency is clearly seen. Notice that the axis are chosen so the excitation frequency is seen clearly linear. For the nonlinear case, higher harmonics, as a multiple of the excitation

frequency, are seen as well. On a magnified plot they are clearly seen to be the third, fifth and seventh harmonics, with decreasing intensity. This is expected for a uneven polynomial stiffness and since the third harmonic is present, it can be concluded that the nonlinear stiffness must be a cubic nonlinearity. Thus MW can, besides showing that nonlinearity is present, help estimating the type of nonlinearity. The participation factor of each of the higher harmonics is computed in section **??**. Fig **??**(d) shows the FT of the linear and nonlinear system. As stated, the FT fails to capture the changing frequency content of the nonlinear system.

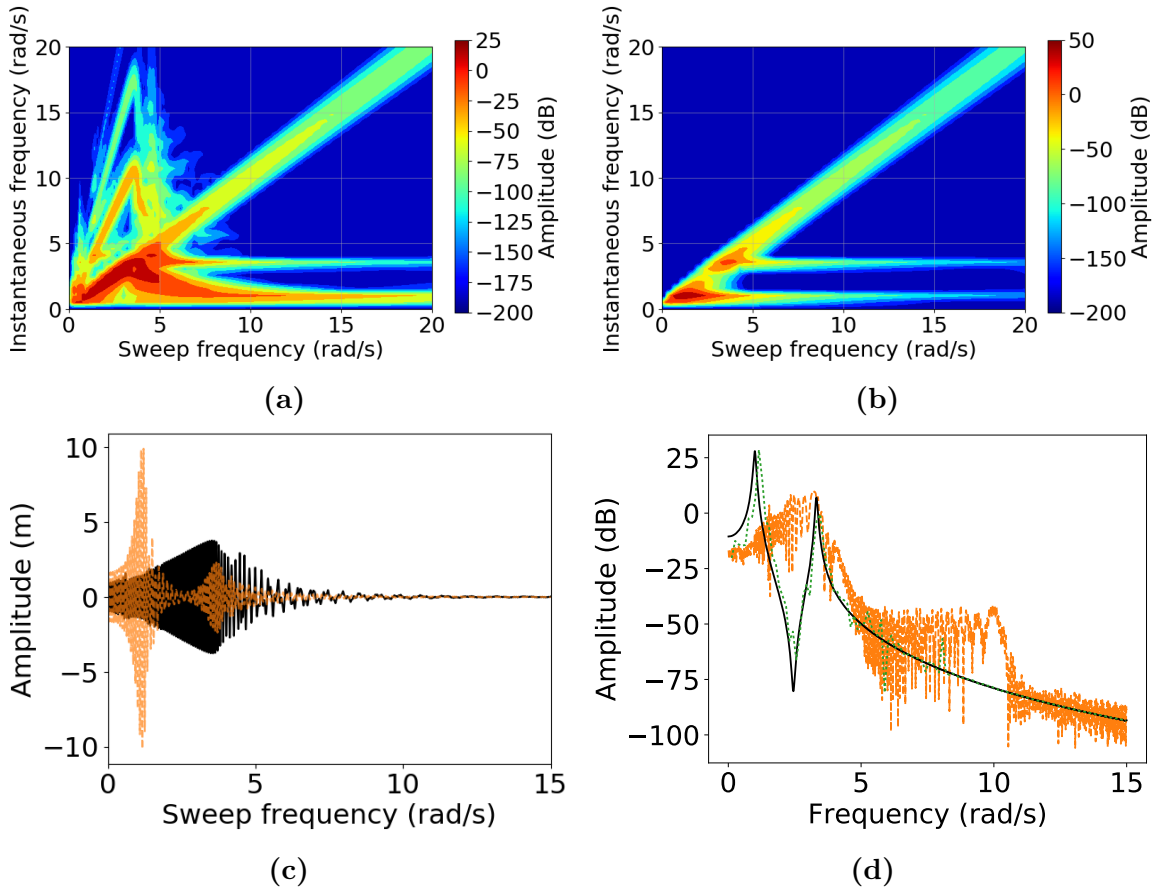

Figure 2.1.2: *Morlet wavelet transform of a sine sweep of the coupled duffing system. Shown for x_1.* ***(a)****: MW of the nonlinear system;* ***(b)****: MM of the underlaying linear system;* ***(c)****: Sine sweep of ——(nonlinear) and - - - -(linear) system;* ***(d)****: Fourier transform of the ——(nonlinear) and - - - -(linear) system. ·····(nonlinear multisine) is the FRF of a multisine excitation of the nonlinear system.*

Summary

The WM shows the instantaneous frequency content of a time signal. Varying frequency content is a sign of nonlinear vibration and the way the spectra changes might give clues to the type of nonlinearity. The frequency spectra is changed in the following way by nonlinear components:

- *Dissipative NLs* does not affect the resonance frequencies much.

- *Hardening (softening) elastic NLs* increase (softens) the resonance frequencies with amplitude.
- *Assymmetric elastic NLs* generate even harmonic components.
- *Symmetric elastic NLs* generate uneven harmonic components.
- *Nonsmooth elastic NLs* generates wideband frequency components.

2.2 Restoring Force Surface

The restoring force surface (RFS) method, introduced by [20] and covered in details in [34], have previously been used as a parameter estimation technique, but is only used as a visual tool for characterization the functional form of the nonlinearity in this report.

If RFS is used for parameter estimation, an estimation of the inertia for the system is needed. This either requires an FE model or, for more than a few DOFs, an complicated algebraic model. If an FE model is used, a low level test campaign could be used to calibrate the model until it fits the experimental eigenfrequencies.

([21] demonstrates a generalisation of the RFS which estimates parameters exclusively from time signals, but the method is only applicable to systems with a few DOFs since the method still consist of direct fitting of Newton's second law.)

The starting point is Newton's second law of dynamics written for a specific DOF located next to a nonlinear structural component

$$\sum_{k=1}^{n} m_{i,k}\ddot{x}_k + g_i(\boldsymbol{x}, \dot{\boldsymbol{x}}) = f_i \tag{2.2.1}$$

where i is the DOF of interest, n the number of DOFs in the system, m_{ik} the mass matrix elements, $\boldsymbol{x}$, $\dot{\boldsymbol{x}}$ and $\ddot{\boldsymbol{x}}$ the displacement, velocity and acceleration vectors, respectively, $\boldsymbol{g}$ the restoring force vector encompassing elastic and dissipative effects, and $\boldsymbol{f}$ the external force vector.

The difference between the traditional usage of RFS, to this approach is to discard any restoring force or inertia terms that are not directly connected to the nonlinear component. (*The discarded terms are generally unknown terms which are practically impossible to measure in an experiment, such as the coupling inertia coefficients and the rotational DOF.*)

If j denote another measured DOF located across the nonlinear connection, see figure **??**, a new formulation of (**??**), which accounts for the difference in displacement and velocity between the selected DOFs, is approximated with

$$m_{i,j}\ddot{x}_i + g_i(x_i - x_j, \dot{x}_i - \dot{x}_j) \approx f_i \tag{2.2.2}$$

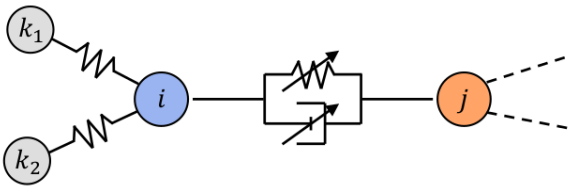

Figure 2.2.1: *Nonlinear connection between node i and j. The linear connections to $k_{1,2}$ are discarded.*

It is further assumed that no external force is applied directly at DOF i (eg. the external force is applied at a different location on the structure), an rearrangement leads to

$$g_i(x_i - x_j, \dot{x}_i - \dot{x}_j) \approx -m_{i,j}\ddot{x}_i \tag{2.2.3}$$

Thus by dropping the constant mass, the nonlinearities can be visualized as the negative acceleration at one side of the connection, as a function of the relative displacement and velocity across this connection. From this an adequate mathematical model can be found.

The shape of g is visualized by plotting the triplet $(x_{i,k} - x_{j,k}, \dot{x}_{i,k} - \dot{x}_{j,k}, \ddot{x}_{i,k})$, where k is the k'th sampled instant. The form of elastic (dissipative) nonlinearities in the connection is visualized by making a slice along the axis of the zero velocity (displacement) of the restoring force surface plot. Either prior knowledge about the physics or a least square fit can be used to find the functional that best represent the nonlinearity.

The major limitations of the RFS method is

- Requires the nonlinear dynamics to be excited
- Shows the total restoring force:
  - with multiple nonlinearities it is not possible to distinguish them uniquely.
  - If the nonlinear force is of the same magnitude as the linear force, it might be necessary to remove a linear trend from the RFS to visualise the nonlinear force.
- Works best swept-sine excitation.
- Damping characterisation is difficult due to the low numerical magnitude.

Example

Using a sine sweep excitation on the coupled duffing system and the RFS methodology,

$$g_i(x_i - x_j, \underbrace{\dot{x}_i - \dot{x}_j}_{<\text{tol}}) \approx -\ddot{x}_i \tag{2.2.4}$$

where *tol* determines the slice thickness, the restoring force is visualised in figs **??** and **??** for x_0 and x_1. A hardening stiffness is seen, without any offset, which correspond to a uneven nonlinear polynomial stiffness. In this case a third order polynomial for both DOFs.

Summary

The RFS provides a direct visualization of the nonlinear stiffness and, to lesser extend, damping curve using a SDOF simplification of the EOMs. The steps are:

- Instrument the nonlinear connection with two accelerometers and use swept sine excitation.
- Integrate and filter to obtain displacement and velocity.
- Calculate the 3D acceleration surface over a single connection.
- Make surface slides to obtain stiffness and damping curve.

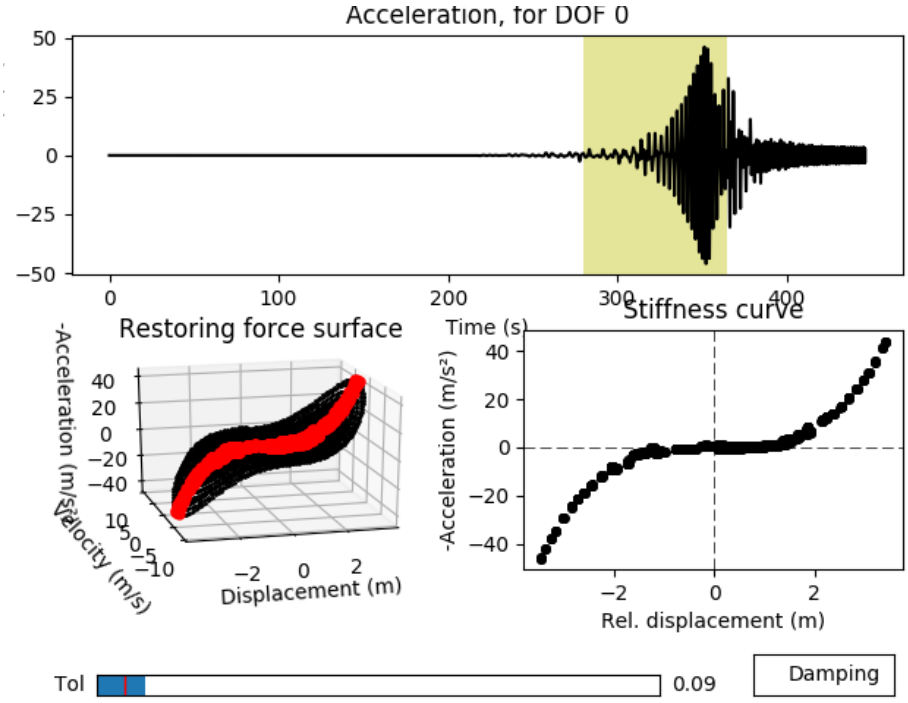

Figure 2.2.2: *Interface for selecting the part of the signal used for visualising the restoring force of the coupled duffing system. Here shown for x_1.* ***upper****: The relevant part of the signal is selected by dragging or resizing the yellow rectangle;* ***left****: Restoring force surface for the selected part of the signal. The red line shows the slice;* ***right****: The visualised stiffness. The slice thickness can be changed by dragging the tolerance slider. Damping is visualised by clicking on damping.*

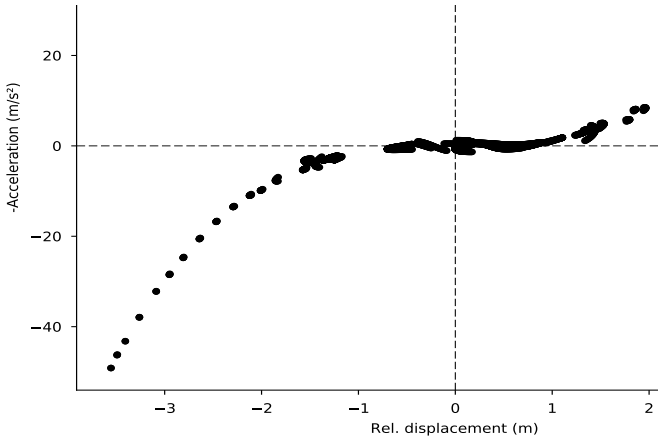

Figure 2.2.3: *The visualised stiffness for x_2 from the coupled duffing system. The figure is extracted from the interface shown in fig.* **??***; just for x_2 instead*

The advantages of RFS as presented here, is that it relies exclusively on measured time series and have a visual understanding. It is not commonly used for parameter estimation for MDOF systems, due to the need for direct fitting of Newton's second law.

The RFS method have been used for estimation of MDOF systems in [8] and [26,

chap. 1.5.1]. But in the former, the complete mass, damping and stiffness matrices are known from a detailed FE model and in the latter, the complete equation of motion for the MDOF system has to be derived a priory to the estimation.

The success of parameter estimation step is conditional upon an accurate characterization of all observed nonlinearities. RFS is also called Accelerated Surface Method (ASM) at times in literature.

2.3 Frequency-domain subspace identification

This section describes a methods for estimation of the underlying linear frequency response function and nonlinear coefficients for nonlinear systems. The method is an (nonlinear) extension of linear subspace methods which are able to deal with multiple-input, multiple-output(MIMO) systems.

The nonlinear subspace methods interpret nonlinearities as unmeasured internal forces, ie. nonlinearities are seen as cause of distortion on the linear FRF matrix. Two main nonlinear methods exist, one in time domain: time-domain subspace identification (TNSI)[19] and one in frequency domain: frequency-domain subspace identification (FNSI)[24] . Both performs equally well in identification and robustness, but the main benefit of FNSI is that the input time series, when converted to frequency domain, can be truncated to a frequency interval of interest and thus reduce the computational time. FNSI is the method used here.

Given the equation of motion for a dynamical system with nonlinearities:

$$\boldsymbol{M}\ddot{\boldsymbol{q}}(t) + \boldsymbol{C}\dot{\boldsymbol{q}}(t) + \boldsymbol{K}\boldsymbol{q}(t) + \boldsymbol{f}_{nl}\left(\boldsymbol{q}(t), \dot{\boldsymbol{q}}(t)\right) = \boldsymbol{p}(t) \tag{2.3.1}$$

where $\boldsymbol{M}$, $\boldsymbol{C}$ and $\boldsymbol{K} \in \mathbb{R}^{n\times n}$ are the mass, linear viscous damping and linear stiffness matrices; $\boldsymbol{q}(t)$ and $\boldsymbol{p}(t) \in \mathbb{R}^n$ are the generalised displacement and external force vectors; $\boldsymbol{f}_{nl}(t) \in \mathbb{R}^n$ is the essentially nonlinear, i.e. nonlinearisable, restoring force vector comprising elastic and dissipative contributions; n is the number of DOFs.

The notation of (**??**) assumes that all linear components of the restoring forces in the system are included in the matrices $\boldsymbol{K}$ and $\boldsymbol{C}$. The nonlinear restoring force is expressed by a linear combination of s lumped nonlinearities

$$\boldsymbol{f}_{nl}\left(\boldsymbol{q}(t), \dot{\boldsymbol{q}}(t)\right) = \sum_{i=1}^{s} \mu_i \boldsymbol{b}_i \boldsymbol{g}_i\left(\boldsymbol{q}(t), \dot{\boldsymbol{q}}(t)\right) \tag{2.3.2}$$

where μ_i is the unknown nonlinear coefficient and $\boldsymbol{g}_i\left(\boldsymbol{q}(t), \dot{\boldsymbol{q}}(t)\right)$ is the the corresponding known (identified by eg. RFS) functional form (or basis function). The location of the nonlinearity is specified by the boolean vector, $\boldsymbol{b}_i \in \mathbb{R}^n$.

Moving the nonlinear terms of (**??**) to the right-hand side

$$\boldsymbol{M}\ddot{\boldsymbol{q}}(t) + \boldsymbol{C}_v\dot{\boldsymbol{q}}(t) + \boldsymbol{K}\boldsymbol{q}(t) = -\sum_{i=1}^{s} \mu_i \boldsymbol{b}_i \boldsymbol{g}_i(t) + \boldsymbol{p}(t) \tag{2.3.3}$$

the system may be viewed as the underlying linear system subjected to the external force $\boldsymbol{p}(t)$ and the internal feedback force due to nonlinearities, as shown in figure **??**.

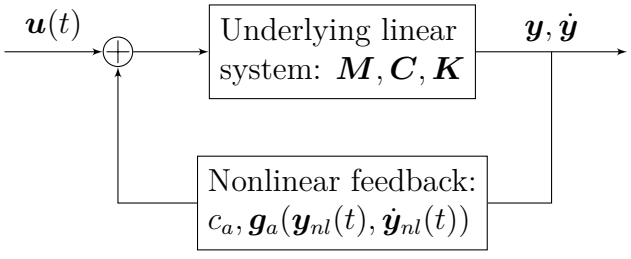

Figure 2.3.1: *Feedback interpretation of nonlinear structural dynamics.*

Using the state vector $\boldsymbol{x} = [\boldsymbol{q}, \dot{\boldsymbol{q}}]^T \in \mathbb{R}^r$, the system (**??**) is rewritten as the state space formulation

$$\begin{aligned} \dot{\boldsymbol{x}}(t) &= \boldsymbol{A}_c \boldsymbol{x}(t) + \boldsymbol{B}_c \boldsymbol{e}(t) \\ \boldsymbol{y}(t) &= \boldsymbol{C}\boldsymbol{x}(t) + \boldsymbol{D}\boldsymbol{e}(t) \end{aligned} \tag{2.3.4}$$

where subscript c denotes $c$ontinuous time and $r = 2n$. $\boldsymbol{e}(t) = \boldsymbol{p}(t)^T, g_1, \ldots, g_s]^T \in \mathbb{R}^{n+s}$ is the extended input vector which concatenates external and nonlinear terms.

State-space and physical matrices have the relations

$$\begin{aligned} \boldsymbol{A}_c &= \begin{bmatrix} \boldsymbol{O}^{r\times r} & \boldsymbol{I}^{r\times r} \\ -\boldsymbol{M}^{-1}K & -\boldsymbol{M}^{-1}\boldsymbol{C} \end{bmatrix} \in \mathbb{R}^{2r\times 2r}, \\ \boldsymbol{B}_c &= \begin{bmatrix} \boldsymbol{0}^{r\times 1} & \boldsymbol{0}^{r\times 1} & \ldots & \boldsymbol{0}^{r\times 1} & \boldsymbol{0}^{r\times 1} \\ -\mu_1\boldsymbol{M}^{-1}\boldsymbol{b}_1 & -\mu_2\boldsymbol{M}^{-1}\boldsymbol{b}_2 & \ldots & -\mu_s\boldsymbol{M}^{-1}\boldsymbol{b}_S & -\mu_1\boldsymbol{M}^{-1}\boldsymbol{b}_1 \end{bmatrix} \in \mathbb{R}^{(n\times\sigma)} \\ \boldsymbol{C} &= \begin{bmatrix} \boldsymbol{I}^{n\times n} & \boldsymbol{I}^{n\times n} \end{bmatrix} \in \mathbb{R}^{(n\times n)} \quad \boldsymbol{D} = \boldsymbol{0}^{n\times\sigma} \end{aligned} \tag{2.3.5}$$

The state matrices are: $\boldsymbol{A}$ and $\boldsymbol{B}$ the input and nonlinear coefficients matrix, the output matrix $\boldsymbol{C}$ and the direct feed through matrix $\boldsymbol{D}$.

This way of characterizing the system above is the same as with TNSI. Using a Fourier transform, the system is

$$\begin{aligned} z_k \boldsymbol{X} &= \boldsymbol{A}_d \boldsymbol{X}(k) + \boldsymbol{B}_d \boldsymbol{E}(k) \\ \boldsymbol{Y}(k) &= \boldsymbol{C}\boldsymbol{X}(k) + \boldsymbol{D}\boldsymbol{E}(k) \end{aligned} \tag{2.3.6}$$

where $z_k = e^{(2i\pi k/N_s)}$ is the Z-transform variable for discrete time models and N_s the number of recorded samples in the time series. $\boldsymbol{X}, \boldsymbol{Y}$ and $\boldsymbol{E}$ are the discrete Fourier transforms of $\boldsymbol{x}, \boldsymbol{y}$ and $\boldsymbol{e}$.

Noget om at fitte en discrete time model til continuous time for sikre good conditioning

The output-state-input equation

The extended input $\boldsymbol{E}$ and output $\boldsymbol{Y}$ is known. The system matrices $\boldsymbol{A}_d, \boldsymbol{B}_d, \boldsymbol{C}$ and $\boldsymbol{D}$ needs to be determined along with the system order r. Frequency-domain subspace methods estimates these matrices based on a reformulation of the state-space eqs. (**??**) in matrix form. The matrix of the measured output spectra is

$$\boldsymbol{Y}_i = \begin{bmatrix} \boldsymbol{Y}(1) & \boldsymbol{Y}(2) & \ldots & \boldsymbol{Y}(N) \\ z_1\boldsymbol{Y}(1) & z_2\boldsymbol{Y}(2) & \ldots & z_F\boldsymbol{Y}(N) \\ z_1^2\boldsymbol{Y}(1) & z_2^2\boldsymbol{Y}(2) & \ldots & z_F^2\boldsymbol{Y}(N) \\ \vdots & & & \\ z_1^{i-1}\boldsymbol{Y}(1) & z_2^{i-1}\boldsymbol{Y}(2) & \ldots & z_F^{i-1}\boldsymbol{Y}(N) \end{bmatrix} \tag{2.3.7}$$

which by defining $\xi = \mathrm{diag}(z_1, z_2, \ldots, z_N)$ is recast to

$$\begin{aligned} \boldsymbol{Y}_i &= \begin{bmatrix} \boldsymbol{Y}^T & (\boldsymbol{Y}\xi)^T & \ldots & (\boldsymbol{Y}\xi^{i-1})^T \end{bmatrix}^T \\ \boldsymbol{E}_i &= \begin{bmatrix} \boldsymbol{E}^T & (\boldsymbol{E}\xi)^T & \ldots & (\boldsymbol{E}\xi^{i-1})^T \end{bmatrix}^T \end{aligned} \tag{2.3.8}$$

where i is the user-defined number of block rows in $\boldsymbol{Y}_i$ and N the number of frequency lines used for identification.

Introducing the extended observability matrix

$$\boldsymbol{\Gamma}_i = \begin{bmatrix} \boldsymbol{C}^T & (\boldsymbol{CA})^T & \dots & (\boldsymbol{CA}^{i-1})^T \end{bmatrix}^T \tag{2.3.9}$$

and the lower-block triangular Toeplitz matrix

$$\boldsymbol{H}_i = \begin{bmatrix} \boldsymbol{D} & \boldsymbol{0} & \boldsymbol{0} & \dots & \boldsymbol{0} \\ \boldsymbol{CB} & \boldsymbol{D} & \boldsymbol{0} & \dots & \boldsymbol{0} \\ \boldsymbol{CAB} & \boldsymbol{CB} & \boldsymbol{D} & \dots & \boldsymbol{0} \\ \vdots & & & & \\ \boldsymbol{CA}^{i-2}\boldsymbol{B} & \boldsymbol{CA}^{i-3}\boldsymbol{B} & \boldsymbol{CA}^{i-3}\boldsymbol{B} & \dots & \boldsymbol{D} \end{bmatrix}^T \tag{2.3.10}$$

By recursive use of eq. (**??**) [24], the output-state-input matrix equation, which is used for estimation in the subspace method, is obtained

$$\boldsymbol{Y}_i = \boldsymbol{\Gamma}_i \boldsymbol{X} + \boldsymbol{H}_i \boldsymbol{E}_i \tag{2.3.11}$$

Estimation of state matrices

The subspace method is applied to eq. (**??**) in order to estimate $\boldsymbol{\Gamma}_i$ and the system order n_s. When $\boldsymbol{\Gamma}_i$ is estimated, the state matrices of eq. (**??**) are extracted and calculated.

The method have two main steps:

- Eliminate the term depending on nonlinearities and forces in eq. (**??**). This is done by projecting the equation onto the orthogonal complement of $\boldsymbol{E}_i$,

  $$\boldsymbol{Y}_i / \boldsymbol{E}_i^{\perp} = \boldsymbol{\Gamma}_i \boldsymbol{X} / \boldsymbol{E}_i^{\perp} = \mathcal{P} \tag{2.3.12}$$

  The geometrical interpretation of this is shown in figure **??** for the 2d case.

  Γ_i is then estimated from a singular value decomposition(SVD) of the projection $\mathcal{P}$

- When Γ_i is estimated, the four state space matrices $(\boldsymbol{A}, \boldsymbol{B}, \boldsymbol{C}, \boldsymbol{D})$ are calculated. See figure **??** for a overview and [24] for more details.

Three assumptions are assumed to be fulfilled for the subspace methods,

1. All the linear modes of vibration in the frequency band of interest are excited or, alternatively, they are all observable in input-output data.

2. The row space of the states $\boldsymbol{X}$ and of the extended input spectra matrix $\boldsymbol{Y}_i$ does not share information,

   $$\text{span}_{\text{row}}(\boldsymbol{X}) \cap \text{span}_{\text{row}}(\boldsymbol{E}_i) = 0$$

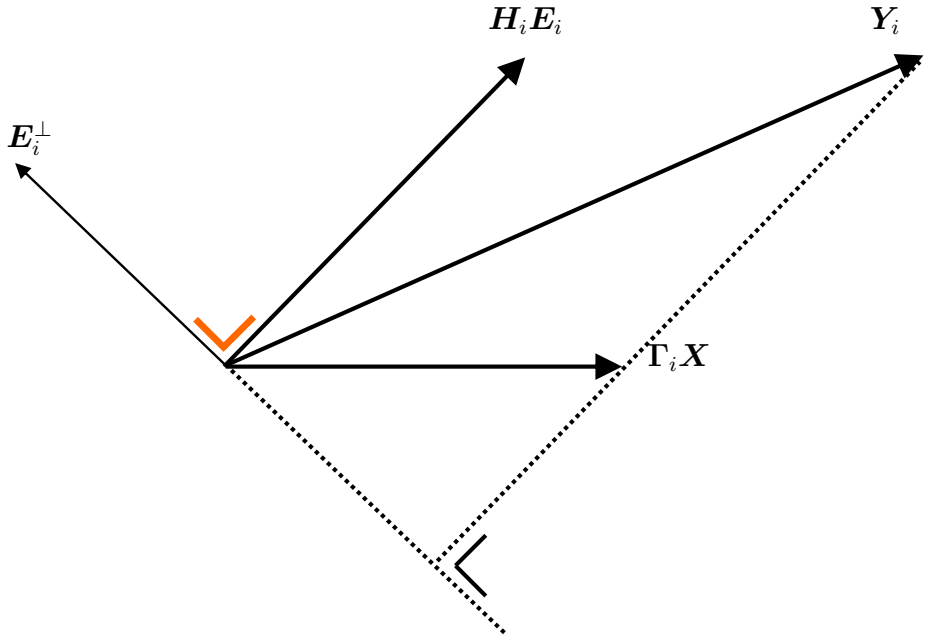

Figure 2.3.2: *Geometric interpretation of eq.* (**??**) *in two dimensional space. The orthogonal complement of* $\boldsymbol{E}_i$*,* $\boldsymbol{E}_i^{\perp}$*, is the set of all vectors that are orthogonal to every vector of* $\boldsymbol{E}_i$ *(thus it is also the null space of* $\boldsymbol{E}_i$*). In the 2d case,* $\boldsymbol{E}_i^{\perp}$ *is simply the vector perpendicular to* $\boldsymbol{E}_i$*, and the projection of* $\boldsymbol{Y}_i$ *cancels the extended input term* $\boldsymbol{H}_i\boldsymbol{E}_i$*. In 3d the orthogonal complement of the plane spanned of two vectors* $\boldsymbol{u}$ *and* $\boldsymbol{v}$*, is the subspace formed by all normal vectors to that plane.*

3. The extended inputs $\boldsymbol{E}_i$ are of full rank, i.e.,

$$\text{rank}(\boldsymbol{E}_i) = \sigma i$$

   Excitations and the nonlinearities have to be such that the inversion of the problem is well-posed

To expand on the second assumption: The state term $\boldsymbol{AX}$ contains linear stiffness and damping information. If constant and/or linear terms are introduced in the nonlinear basis functions, the intersection between the states and the extended inputs $\boldsymbol{E}_i$ is no longer empty, which violate the assumption. This requires nonlinear basis functions to be nonlinearisable, i.e. they should be zero and have zero slope at the origin.

Dimension:

$\boldsymbol{b}_s \in \mathbb{R}^l$ is a boolean vector specifying the location of the nonlinearity μ_s. $\sigma = m+s$, where s is the number of lumped nonlinearities and $m \leq r$ is the number of $m$easured applied forces. $l \leq r$ is the number of $m$easured applied displacement. n is the model order, not $n = 2r$ as used in the beginning of the article, and r is number of DOFs.

Types of nonlinear functional

As stated, the nonlinear basis functions should be zero and have zero slope at the origin. For continuous nonlinear restoring force, polynomial functions with order chosen from RFS-plots can be used. For discontinuous systems, e.g. contact polynomials

might not be well suited, for instance higher order polynomials exhibit oscillations around the origin. An alternative is to use piecewise cubic spines instead. Even if they cannot realise a perfect fitting (they are continuous by nature), they are appropriate for representing sudden events, like sharp changes in stiffness/damping curves.

In order to get the basis functions from cubic splines, the abscissas of knots is specified on beforehand and the ordinate as free parameters. FNSI then estimate the ordinate. Choosing the number of knots and their abscissas should rigorously be sought by minimising the difference in some metric between the predictions of the non-linear model and measured data. In reality it is still done by trial and error.

Using cubic splines might be termed *gray box* identification where using polynomials is *white box*. The difference is that with gray box, the nonlinearities are described by functionals that may represent a vast variaty of nonlinear behaviour and thus requiring less specific knowledge of the underlying physics.

Estimating model order

In the presence of non-linearities, the model order translates the number of underlying linear modes excited in the output data. This implies that, similarly to linear system identification, a stabilisation analysis can be utilised as decision-making tool instead of looking at the singular values of $\boldsymbol{S}$, (**??**). The stabilisation diagram shows the stabilisation of the estimated linear parameters: stabilisation in frequency, stabilisation in damping and stabilisation of the mode. If all three parameters are stabilised the mode is full stabilised. Stabilisation is compared to the same mode for one model order higher. Stabilisation for the mode is calculated by the modal assurance criterion(MAC) [1],

$$MACX(r,q) = \frac{|\boldsymbol{\psi}_r^T \boldsymbol{\psi}_q^*|^2}{(\boldsymbol{\psi}_r^T \boldsymbol{\psi}_r^*)\left(\boldsymbol{\psi}_q^T \boldsymbol{\psi}_q^*\right)} \tag{2.3.16}$$

If the model order is chosen too low, it will result in unmodelled dynamics, whereas too large orders lead to overmodelling issues such as an increase of the noise sensitivity of the model. It should be noted that model selection requires that adequate basic functions are used.

Without anticipating the example, a stabilisation diagram for the coupled duffing system is shown in figure **??** along with singular values of $\boldsymbol{S}$ in figure **??**. The two modes are clearly seen. From the stabilisation diagram a model order of four is chosen. This gives stabilisation in the linear parameters. The plot of the singular values shows a jump of six orders magnitude between model order four and five, verifying the chosen model order. In general only the stabilisation diagram is used; the singular value plot is only used if a stabilisation diagram is not implemented.

The determination of the model order is very simple and clear here. For larger system this might not be the case, as seen with the more involved examples in section **??**.

Example

Figure **??** shows the periodicity of the recorded signal. The signal of the last recorded period is compared to previous periods. For identification, multiple periods can be used but transient effects should not be present; which is indicated by a low periodicity.

The estimation of the nonlinear parameters of the coupled duffing system is shown in figure **??** for model order four. The variation of the real part ofμ is shown in a 1% interval, with very little frequency dependency in the frequency range of interest. The imaginary part is about three orders of magnitude smaller. Both indicates a good quality of the estimation. The spectral averages are

$$\begin{aligned} \mathrm{Re}(\mu_1) &= 1.000, \quad \mathrm{Im}(\mu_1) = 1.09 \times 10^{-4} \\ \mathrm{Re}(\mu_2) &= 1.000, \quad \mathrm{Im}(\mu_1) = 7.73 \times 10^{-4} \end{aligned} \tag{2.3.17}$$

matching the simulated values well.

The FNSI method also estimate the underlaying linear properties. As seen from table **??**, the linear parameters are identified correctly. Ensuring that linear parameters are identified, also shows that nonlinear coefficients are identified correct.

Mode	Frequency (rad/s)	Damping ration (%)
1	1.00	5.00
2	3.32	1.51
1	1.19	3.96
2	3.40	1.41

Table 2.3.1: *Estimated linear natural frequencies and damping ratios for the coupled Duffing system.* ***(upper)****: Nonlinear identification with FNSI;* ***(lower)****: Linear identification*

Figure **??** shows the transfer function. The linear transfer function found by FNSI match the theoretical linear transfer function.

Estimation error

It seems that the FNSI method works quite well - both nonlinear and linear parameters are estimated with high accuracy - and indeed it does work well. But it is not exact, as will be shown here: the method introduce spurious undesired terms, and even if they are small in magnitude, they still alters the identified model.

Summary

The FNSI method is able to identifying multiple nonlinear parameters for system with many DOFs. It differs from time domain methods, with the ability to truncate measured signals to the frequency intervals of interest making computations faster for large systems.

Characterisation of the nonlinearity is important to get a good identification. If there is limited knowledge about the nonlinearity, cubic splines can be used instead of polynomials. In general the following steps can be used to check the validity of the identification:

- Check the stabilisation of the first mode.
- Check the modal parameters compared to linear identification.
- Check the stability of the nonlinear coefficients versus frequency.
- Check the magnitude of the imaginary parts of the coefficients.

1. Choose the index i and the number of processed frequency lines N
2. Concatenate external forces and nonlinearities to form the extended input spectra E_i
3. Compute the orthogonal projection
$$\mathcal{P} = \boldsymbol{Y}_i / \boldsymbol{E}_i^{\perp}$$
using QR-decomposition.
4. Compute the SVD of $\mathcal{P}$
$$\mathcal{P} = \boldsymbol{U}\boldsymbol{S}\boldsymbol{V} \tag{2.3.13}$$
5. Determine model order n_s from singular values in $\boldsymbol{S}$ or from a stabilisation diagram. Truncate $\boldsymbol{U}$ and $\boldsymbol{S}$ accordingly to define $\boldsymbol{U}_1$ and $\boldsymbol{S}_1$.
6. Estimate the extended observability matrix $\boldsymbol{\Gamma}_i$
$$\hat{\boldsymbol{\Gamma}}_i = \boldsymbol{U}_1 \boldsymbol{S}_1^{1/2}$$
7. Estimate $\boldsymbol{A}$ using the shift property of $\boldsymbol{\Gamma}_i$,
$$\underline{\boldsymbol{\Gamma}_i}\hat{\boldsymbol{A}} = \overline{\boldsymbol{\Gamma}_i} \iff \hat{\boldsymbol{A}} = \underline{\boldsymbol{\Gamma}_i^{+}}\overline{\boldsymbol{\Gamma}_i}$$
where $\underline{\boldsymbol{\Gamma}_i}$ and $\overline{\boldsymbol{\Gamma}_i}$ are the matrix $\boldsymbol{\Gamma}_i$ without its first and last l rows. $\boldsymbol{C}$ is extracted as the first block row of $\boldsymbol{\Gamma}_i$.
8. Estimate $\boldsymbol{B}$ and $\boldsymbol{D}$ by defining the transfer function matrix $\boldsymbol{G}_s$,
$$\boldsymbol{G}_s(k) = \boldsymbol{C}(z_k \boldsymbol{I} - \boldsymbol{A})^{-1}\boldsymbol{B} + \boldsymbol{D}$$
and minimise the difference between the measured and modelled output spectra in a linear least square sense, i.e.
$$\hat{\boldsymbol{B}}, \hat{\boldsymbol{D}} = \arg\min_{\boldsymbol{B},\boldsymbol{D}} \sum_{k=1}^{F} |\boldsymbol{Y}(k) - \boldsymbol{G}_s(k)\boldsymbol{E}(k)|^2$$
9. Convert $\boldsymbol{A}, \boldsymbol{B}, \boldsymbol{C}$ and $\boldsymbol{D}$ into continuous-time matrices and form the extended FRF $\boldsymbol{H}^e(\omega)$.
$$\boldsymbol{H}^e(\omega) = \boldsymbol{C}_c \left(j\omega \boldsymbol{I}^{n\times n} - \boldsymbol{A}_c\right)^{-1} \boldsymbol{B}_c^e + \boldsymbol{D}_c^e \in \mathbb{C}^{(l\times\sigma)} \tag{2.3.14}$$
10. Estimate the nonlinear coefficients μ_j and the linear FRF matrix $\boldsymbol{H}(\omega)$. The FRF matrix of the underlying linear system $\boldsymbol{H}(\omega) \in \mathbb{C}^{(l\times l)}$ and the nonlinear coefficients μ_s are found from (**??**) as
$$\boldsymbol{Q}(\omega) = \boldsymbol{H}(\omega)\left\{\boldsymbol{I}^{l\times 1} \quad -\mu_1\boldsymbol{b}_1 \quad \ldots \quad -\mu_s\boldsymbol{b}_s\right\}\boldsymbol{E}(\omega) = \boldsymbol{H}^e(\omega)\boldsymbol{E}(\omega) \tag{2.3.15}$$

Figure 2.3.3: *Overview of the FNSI methodology*

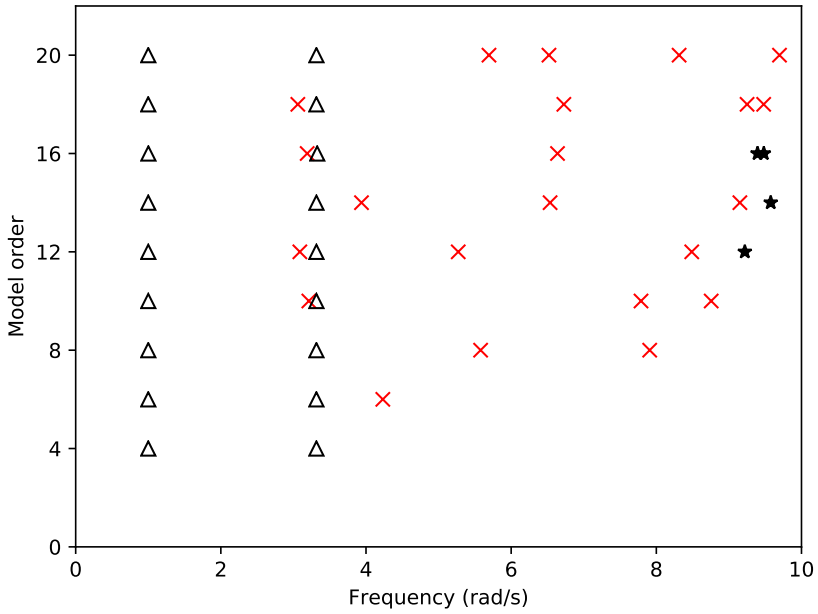

Figure 2.3.4: *Estimation of model order. Stabilisation diagram with linear FRF overlayed.* × *(red): new pole;* ⋆*: stabilisation in natural frequency;* □*: extra stabilisation in damping ratio;* ∘*: extra stabilisation in MACX;* △*: full stabilisation. Stabilisation thresholds in natural frequency, damping ratio and MACX value are* $0.5\%, 2\%, 0.98$*, respectively. Not all types of stabilisation are present here.*

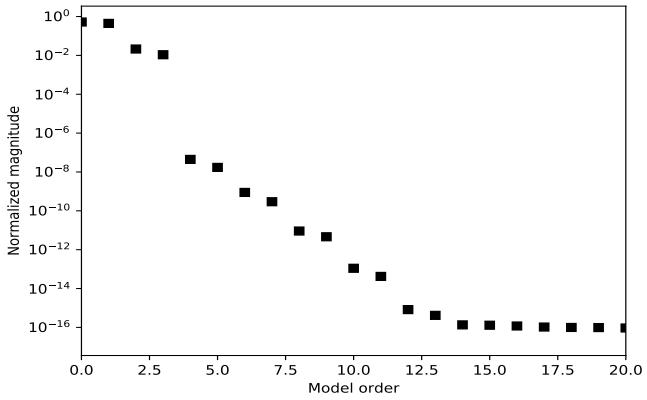

Figure 2.3.5: *First tventy singular values. A jump of six orders magnitude is seen between model order four and five.*

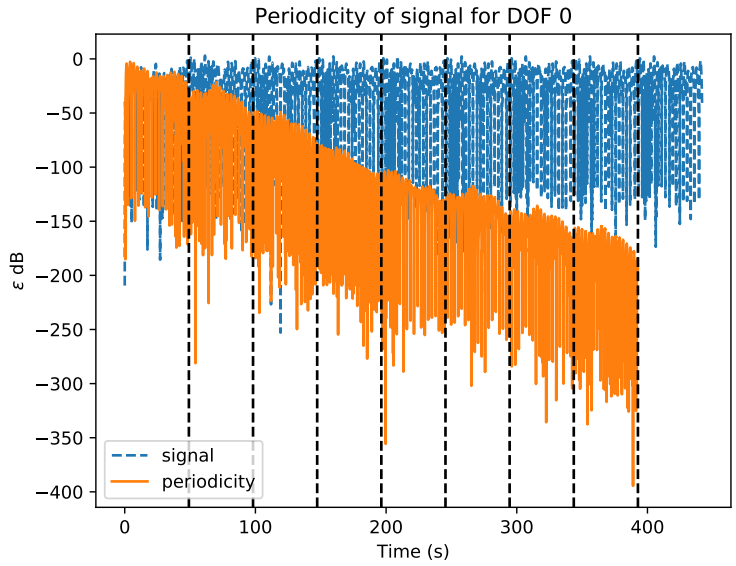

Figure 2.3.6: *Periodicity of recorded signal at DOF 0. Vertical lines indicate periods. A low periodicity shows that transient effects have died out*

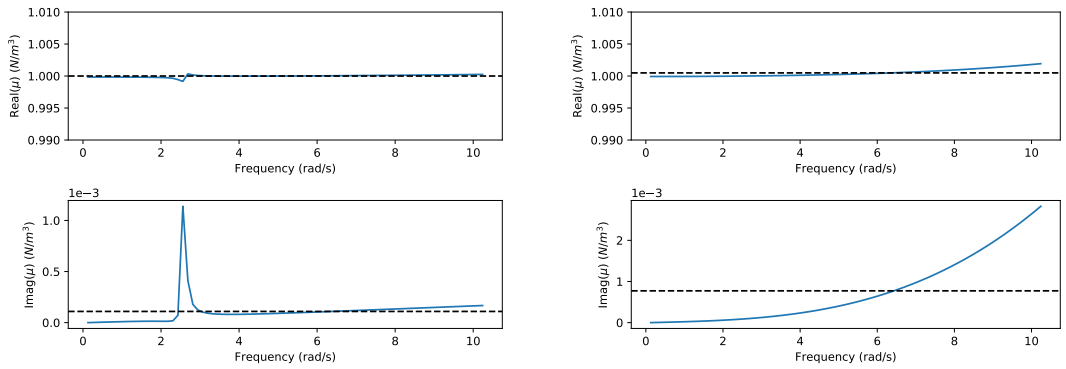

(a) **(b)**

Figure 2.3.7: *Real and imaginary part of estimated nonlinear coefficients μ_1 and μ_2. The variation of Re(μ) is shown in a 1% interval, with very little frequency dependency in the frequency range of interest. The imaginary part is about three orders of magnitude smaller. Both indicates a good quality of the estimation.* ***(a)****: μ_1;* ***(b)****: μ_2.*

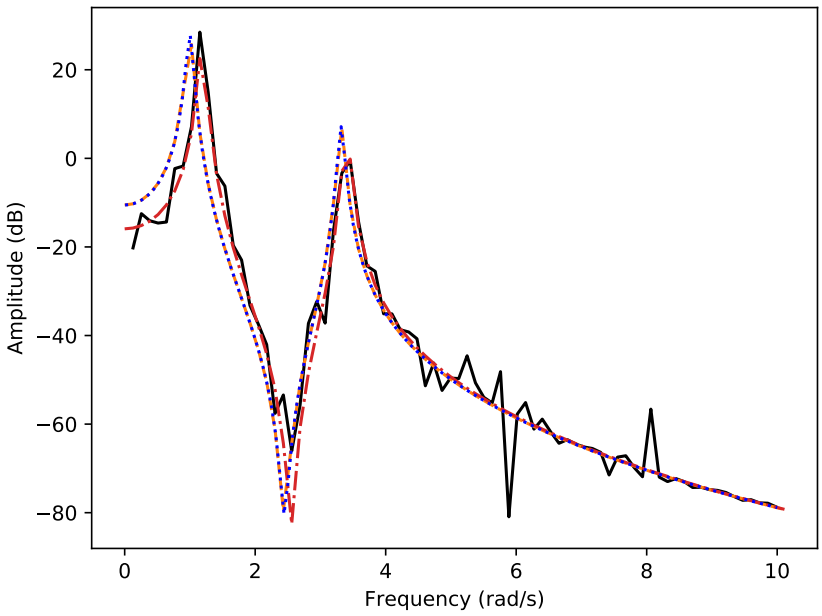

Figure 2.3.8: *Transfer function H_1 for the coupled duffing system. ——(black): H1 from signal; – – –(red): Linear identified; - - - -(orange): Linear identified from FNSI; ·····(blue): Theoretical linear*

Chapter 3

From identification to design

This chapter deals with the prediction of behaviour of nonlinear system, after nonlinear components have been determined. Paraphrased it could be called *virtual prototyping*. Here methods to detect bifurcations, stability and internal resonance are presented. The long-term ambition is to use this knowledge to improve design, taking nonlinear behaviour into account.

This chapter represent a change of methodology. Where the methods for identification in the previous chapter relied exclusively on time signals, the methods of this chapter relies exclusively on FE models. An natural extension, where the information from identification is used to build an accurate computer model. By accurate model, is meant a model where the n lowest eigenfrequencies match the experimental ones.

Two methods are treated: Harmonic balance(HB) continuation, used for detecting and identifying bifurcations, and nonlinear normal modes(NNM) continuation, used to detect internal resonance.

Måske til opsummering: (This is a step forward from the traditional methods used today where designs are based on shaping resonance(by solving eigenvalue problems) and validated with modal responses from experimental data.)

3.1 Periodic solution

Before turning to the methods themselves, a few concepts must be revisited. Computing the periodic solution of a nonlinear system means searching for a solution $\boldsymbol{x}$ to

$$\boldsymbol{M}\ddot{\boldsymbol{x}}(t) + \boldsymbol{C}\dot{\boldsymbol{x}}(t) + \boldsymbol{K}\boldsymbol{x}(t) + \boldsymbol{f}_{nl}\left(\boldsymbol{x}(t), \dot{\boldsymbol{x}}(t)\right) = \boldsymbol{p}(t) \tag{3.1.1}$$

that satisfies a periodicity condition

$$\boldsymbol{x}(t+T) = \boldsymbol{x}(t) \tag{3.1.2}$$

where T is the period. This is a boundary value problem(BVP). By periodic solution, steady state conditions are implied. Stability of the periodic solution will also be addressed.

There are at least three ways to describe such a periodic solution.

- Provide initial condition $[\boldsymbol{x}_0\dot{\boldsymbol{x}}_0]$ and the period T. Then do time integration over T.
- Use piecewise polynomial functions and the period T
- Use Fourier series and the period T

In this section, the methods for finding the first and last representations of a periodic solution is described. They are denoted the shooting method and harmonic balance method respectively. The one not covered here is called Orthogonal collocation. The shooting method is used as part of calculating NNMs and harmonic balance is used for bifurcation analysis. Both methods could be used for both tasks, but there are significant numerical benefits for using them as here.

Shooting method

The shooting method works by finding, in an iterative way, the initial state $\boldsymbol{z} = [\boldsymbol{x}, \dot{\boldsymbol{x}}]^T$ and period T that describes a periodic motion, see Nayfeh and Balachandran [23] for more details.

One start by guessing on periodic steady state(ie. initial state and period) and then *shoots* forward one period with the hope of arriving close to the guessed initial state. The difference between the initial and final states is used to correct the initial state, and the method *shoots* forward another period and continue until final and initial state match. The final state is found by integration, see appendix **??** for details on the nonlinear Newmark integration. The corrections are done by Newton-Rahpson iterations.

The EOM (**??**) is recast into state space form. Since this method is used for NNMs, it is recast in the undamped and unforced form.

$$\dot{\boldsymbol{z}} = \boldsymbol{g}(\boldsymbol{z}) = \begin{bmatrix} \dot{\boldsymbol{x}} \\ -\boldsymbol{M}^{-1}(\boldsymbol{K}\boldsymbol{x} + \boldsymbol{f}_{nl}) \end{bmatrix} \tag{3.1.3}$$

A solution $\boldsymbol{z}_p(t, \boldsymbol{z}_{p0})$ is a solution of the autonomous system eq. (**??**) if $\boldsymbol{z}_p(t, \boldsymbol{z}_{p0}) = \boldsymbol{z}_p(t + T, \boldsymbol{z}_{p0})$ where T is the minimal period. Thus the periodic condition is

$$\boldsymbol{H}(\boldsymbol{z}_{p0}, T) \equiv \boldsymbol{z}(T, \boldsymbol{z}_{p0}) - \boldsymbol{z}_{p0} = \boldsymbol{0} \tag{3.1.4}$$

$\boldsymbol{H}$ is called the shooting function.

To make the solution $\boldsymbol{z}(t)$ uniquely defined, the phase must be fixed. If $\boldsymbol{z}(t)$ is a solution to (**??**) then $z(t+\Delta t)$ is geometrically the same solution in state space for any Δt. Ie. the initial condition $\boldsymbol{z}_{p0}$ can be arbitrarily chosen anywhere on the periodic solution. To prevent this, a phase condition $h(\boldsymbol{z}_{p0}) = 0$ is set as a additional condition. Most phase conditions imposes one of the unknowns to be set to 0, e.g. the initial displacement or velocity of a DOF(often velocity). For NNM computations specific, other phase conditions will reduce the computation complexity as will be mentioned in section **NNM**. See figure **??** for a illustration of different phases for the periodic solution. **ER DET ET RELEVANT PLOT? JEG SYNES TEKSTEN ER NOK.**

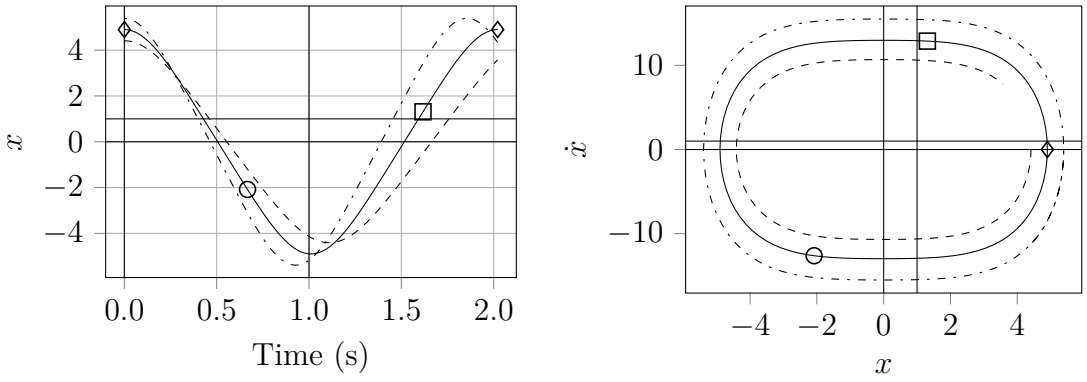

Figure 3.1.1: *Solution of the duffing eq. $\ddot{x}+x+0.5x^3 = 0$ for different initial conditions and $T = 2.0215s$. a): time series; b): phase space. Initial conditions for different line styles: —: [4.9009, 0]; − − −: 0.9*[4.9009, 0]; − · − · −·: 1.1*[4.9009, 0]; Markers represent different initial conditions for the periodic solution. ⋄: [4.9009, 0]; □: [1.308, 12.8764]; ∘: [-2.0825, -12.6177]*

In summary, the periodic solution is found by solving

$$\begin{cases} H(\boldsymbol{z}_{p0}, T) = 0 \\ h(\boldsymbol{z}_{p0}) = 0 \end{cases} \tag{3.1.5}$$

The corrections to the initial guess is found by Newton-Raphson iterations. The shooting function is expanded in a Taylor series

$$\boldsymbol{H}(\boldsymbol{z}_{p0}, T) + \left.\frac{\partial \boldsymbol{H}}{\partial \boldsymbol{z}_{p0}}\right|_{(\boldsymbol{z}_{p0},T)} \Delta \boldsymbol{z}_{p0} + \left.\frac{\partial \boldsymbol{H}}{\partial T_{p0}}\right|_{(\boldsymbol{z}_{p0},T)} \Delta T + + hot. = 0 \tag{3.1.6}$$

where *hot.* is higher order terms.

Thus the corrections are found by solving the linear equation

$$\begin{bmatrix} \left.\frac{\partial \boldsymbol{H}}{\partial \boldsymbol{z}_{p0}}\right|_{(\boldsymbol{z}_{p0},T)} & \left.\frac{\partial \boldsymbol{H}}{\partial T_{p0}}\right|_{(\boldsymbol{z}_{p0},T)} \\ \left.\frac{\partial h}{\partial \boldsymbol{z}_{p0}}\right|_{(\boldsymbol{z}_{p0},T)} & 0 \end{bmatrix} \begin{bmatrix} \Delta \boldsymbol{z}_{p0} \\ \Delta T \end{bmatrix} = \begin{bmatrix} -\boldsymbol{H}(\boldsymbol{z}_{p0}, T) \\ -h(\boldsymbol{z}_{p0}, T) \end{bmatrix} \tag{3.1.7}$$

since $\boldsymbol{h}_{NNM}$ have the transformation $\mathbb{R}^{\aleph\digamma+\daleth} \rightarrow \mathbb{R}^{\aleph\digamma+\daleth}$ the system above is over determined, ie. the matrix to invert is not square, and is solved in a least square sense.

The state is updated as

$$\boldsymbol{z}_{p0}^{k+1} = \boldsymbol{z}_{p0}^{k} + \Delta \boldsymbol{z}_{p0}^{k}, \quad T^{k+1} = T^{k} + \Delta T^{k} \tag{3.1.8}$$

where k is iteration number. The iteration is stopped when $\boldsymbol{H} = 0$ to some tolerance. Newmark-Raphson is a local algorithm. Convergence is guarantied when the initial guess is close to solution. Otherwise not. The initial guess could for instance be the first linear mode and corresponding period. If the Jacobian matrix is exact, the convergence is second order.

It should be mentioned that for some forcing parameters, where a nonlinear system might have multiple solutions, the NR will, depending on the initial conditions, converge towards only one of them. Methods relying on the homotopy method or Groebner bases can be employed to find multiple solution - not that I know anything about these methods.

Sensitivity analysis

The partial derivatives of the shooting function, used in the NR iterations, are found as:

$$\frac{\partial \boldsymbol{H}}{\partial T} = \left.\frac{\partial \boldsymbol{z}(t, \boldsymbol{z}_0)}{\partial t}\right|_{t=T} = \boldsymbol{g}(\boldsymbol{z}(T, \boldsymbol{z}_0)) \tag{3.1.9}$$

$$\frac{\partial \boldsymbol{H}}{\partial \boldsymbol{z}_0} = \left.\frac{\partial \boldsymbol{z}(t, \boldsymbol{z}_0)}{\partial \boldsymbol{z}_0}\right|_{t=T} - \boldsymbol{I} \tag{3.1.10}$$

$\partial \boldsymbol{H}/\partial T$ is a $2n$ vector. The Jacobian matrix $\partial \boldsymbol{H}/\partial \boldsymbol{z}_0$ is $2n \times 2n$, same as the identity matrix $\boldsymbol{I}$.

The Jacobian matrix $\partial \boldsymbol{z}(t, \boldsymbol{z}_0)/\partial \boldsymbol{z}_0$, which represent the variation of the solution $\boldsymbol{z}(t, \boldsymbol{z}_0)$ at time t when the initial conditions $\boldsymbol{z}_0$ are pertubated, is normally calculated in two ways. Either by finite difference: successively pertubation of each of the $2n$ initial condtion and integrating over the period. This is computationally expensive and gives slower NR convergence since the Jacobi matrix is only approximate.

Instead sensitivity analysis is used. The state space formulation (**??**) is differentiated with respect to initial conditions $\boldsymbol{z}_0$

$$\frac{\partial}{\partial \boldsymbol{z}_0}\left[\dot{\boldsymbol{z}}(t, \boldsymbol{z}_0)\right] = \frac{\partial}{\partial \boldsymbol{z}_0}\left[\boldsymbol{g}(\boldsymbol{z}(t, \boldsymbol{z}_0))\right] \implies \tag{3.1.11}$$

$$\frac{\mathrm{d}}{\mathrm{d}t}\left[\frac{\partial \boldsymbol{z}(t, \boldsymbol{z}_0)}{\partial \boldsymbol{z}_0}\right] = \left.\frac{\partial \boldsymbol{g}(\boldsymbol{z})}{\partial \boldsymbol{z}}\right|_{\boldsymbol{z}(t, \boldsymbol{z}_0)} \frac{\partial \boldsymbol{z}(t, \boldsymbol{z}_0)}{\partial \boldsymbol{z}_0} \tag{3.1.12}$$

with initial condition

$$\frac{\boldsymbol{z}(0, \boldsymbol{z}_0)}{\boldsymbol{z}_0} = \boldsymbol{I} \tag{3.1.13}$$

since $\boldsymbol{z}(0, \boldsymbol{z}_0) = \boldsymbol{z}_0$

Then eq. (**??**) is integrated over T to obtain the Jacobian matrix at time $t = T$. This integration is linear and carried out at the same time as the Newmark integration of the periodic solution. In practise the EOM formulation eq. (**??**) is used for the sensitivity analysis. See appendix **??** for a derivation. The sensitivity analysis requires the nonlinear forces to be smooth. If they are nonsmooth, finite difference have to be used.

Stability

The stability of a periodic solution is found from the Jacobian matrix evaluated at $t = T$, called the *monodromy matrix*

$$\Phi = \left.\frac{\partial \boldsymbol{z}(t, \boldsymbol{z}_0)}{\partial \boldsymbol{z}_0}\right|_{t=T} \tag{3.1.14}$$

It determines whether a small initial perturbation decays or grows. The stability is found from the eigenvalues σ_i, the Floquet multipliers. If an Floquet multiplier is larger than one (i.e., $|\sigma_i| > 1$), the orbit is unstable. Conversely, the periodic orbit is stable if $|\sigma_i \leq 1, \forall i$

Equivalently the Floquet exponents λ could be used. If there is at least one Floquet exponents with a real part larger than 0 the solution is unstable. They are related through the relation

$$\sigma_i = e^{\lambda_i T} \tag{3.1.15}$$

Both variants are depicted on the complex plane and either compared to the unit circle or the imaginary axis, respectively.

Harmonic balance

Where the shooting method finds a periodic solution by solving the system in time domain, HB finds the periodic solution in frequency domain. The method is described in Detroux, Renson, and Kerschen [4]. A periodic solution to the damped and forced EOM eq. (**??**) is sought.

As the signal $\boldsymbol{x}$ and forces $\boldsymbol{f}(\boldsymbol{x}, \dot{\boldsymbol{x}}, \omega, t) = \boldsymbol{p}(\omega, t) - \boldsymbol{f}_{nl}(\boldsymbol{x}\dot{\boldsymbol{x}})$ are assumed periodic, they are approximated by Fourier series truncated to the N_H-th harmonic

$$\boldsymbol{x}(t) = \frac{\boldsymbol{c}_0^x}{\sqrt{2}} \sum_{k=1}^{N_h} (s_k^x \sin(k\omega t) + c_k^x \cos(k\omega t)) \tag{3.1.16}$$

$$\boldsymbol{f}(t) = \frac{\boldsymbol{c}_0^f}{\sqrt{2}} \sum_{k=1}^{N_h} (s_k^f \sin(k\omega t) + c_k^f \cos(k\omega t)) \tag{3.1.17}$$

where $\boldsymbol{s}_k$ and $\boldsymbol{c}_k$ represent the vectors of the Fourier coefficients related to sine and cosine terms. The Fourier coefficients of the force $\boldsymbol{f}(t)$, $\boldsymbol{s}_k^f$ and $\boldsymbol{c}_k^f$ depends on the Fourier coefficients of the displacement $\boldsymbol{x}(t)$, $\boldsymbol{s}_k^x$ and $\boldsymbol{c}_k^x$ which are the new unknowns. Gathering the coefficients into vectors

$$\boldsymbol{z} = \begin{bmatrix} (\boldsymbol{c}_0^x)^T & (\boldsymbol{s}_1^x)^T & (\boldsymbol{c}_1^x)^T & \cdots & (\boldsymbol{s}_{N_H}^x)^T & (\boldsymbol{c}_{N_H}^x)^T \end{bmatrix}^T \tag{3.1.18}$$

$$\boldsymbol{b} = \begin{bmatrix} (\boldsymbol{c}_0^f)^T & (\boldsymbol{s}_1^f)^T & (\boldsymbol{c}_1^f)^T & \cdots & (\boldsymbol{s}_{N_H}^f)^T & (\boldsymbol{c}_{N_H}^f)^T \end{bmatrix}^T \tag{3.1.19}$$

Using a compact notion the displacement and force is written

$$\boldsymbol{x}(t) = (\boldsymbol{Q}(t) \otimes \mathbb{I}_n)\boldsymbol{z} \tag{3.1.20}$$

$$\boldsymbol{f}(t) = (\boldsymbol{Q}(t) \otimes \mathbb{I}_n)\boldsymbol{b} \tag{3.1.21}$$

where $\otimes$ is the Kronecker product, $\mathbb{I}_n$ the identity matrix of size n and $\boldsymbol{Q}$ a vector with harmonic terms

$$\boldsymbol{Q}(t) = \begin{bmatrix} \frac{1}{2} & \sin(\omega t) & \cos(\omega t) & \cdots & \sin(N_H \omega t) & \cos(N_H \omega t) \end{bmatrix} \tag{3.1.22}$$

Velocities and accelerations are found using the Fourier series as

$$\dot{\boldsymbol{x}} = \left(\dot{\boldsymbol{Q}}(t) \otimes \mathbb{I}_n\right)\boldsymbol{z} = \left((\boldsymbol{Q}(t)\boldsymbol{\nabla}) \otimes \mathbb{I}_n\right)\boldsymbol{z} \tag{3.1.23}$$

$$\ddot{\boldsymbol{x}} = \left(\ddot{\boldsymbol{Q}}(t) \otimes \mathbb{I}_n\right)\boldsymbol{z} = \left((\boldsymbol{Q}(t)\boldsymbol{\nabla}^2) \otimes \mathbb{I}_n\right)\boldsymbol{z} \tag{3.1.24}$$

$$\tag{3.1.25}$$

By substituting eqs. (??)-(??) and (??)-(??) into the EOM (??) and using a galerkin procedure, one ends up with the equations of motion in frequency domain (see appendix ?? for more details on the derivation and definition of $\boldsymbol{\nabla}$)

$$(\boldsymbol{\nabla}^2 \otimes \boldsymbol{M})\boldsymbol{z} + (\boldsymbol{\nabla} \otimes \boldsymbol{C})\boldsymbol{z} + (\mathbb{I}_{2N_H} \otimes \boldsymbol{K})\boldsymbol{z} = (\mathbb{I}_{2N_H} \otimes \mathbb{I}_n)\boldsymbol{b} \tag{3.1.26}$$

or in more compact form

$$\boldsymbol{H}(\boldsymbol{z}, \omega) = \boldsymbol{A}(\omega)\boldsymbol{z} - \boldsymbol{b}(\boldsymbol{z}) = \boldsymbol{0} \tag{3.1.27}$$

where $\boldsymbol{A}$ describes the linear dynamics

$$\boldsymbol{A} = \boldsymbol{\nabla}^2 \otimes \boldsymbol{M} + \boldsymbol{\nabla} \otimes \boldsymbol{C} + \mathbb{I}_{2N_H} \otimes \boldsymbol{K} \tag{3.1.28}$$

If z^* is a solution of (??), then the time signal x^* constructed from z^* is periodic and satisfies the eom (??). As with the shooting function, eq. (??) is nonlinear (due to $\boldsymbol{b}$ dependence on $\boldsymbol{z}$) and have to be solved iteratively by Newton-Rahpson iterations. It should however be noted that $\boldsymbol{H}(\boldsymbol{z}, \omega)$ is an (nonlinear) algebraic equation, ie there is no need for integration.

$$\boldsymbol{z}^{(k+1)} = \boldsymbol{z}^{(j)} - \frac{\boldsymbol{H}(\boldsymbol{z}, \omega)}{\boldsymbol{H}_{\boldsymbol{z}}(\boldsymbol{z}, \omega)} \tag{3.1.29}$$

Expression of nonlinear terms and Jacobian matrix

Solution of eq (**??**) requires calculation of $\boldsymbol{H}$ and of the Jacobian matrix $\boldsymbol{H}_{\boldsymbol{z}}$, which in turn requires calculation of $\boldsymbol{b}$ and its derivatives.

It is not known how the Fourier coefficients in $\boldsymbol{b}$ relates to the coefficients in $\boldsymbol{z}$, ie. it is not possible to directly calculate $\boldsymbol{b}(\boldsymbol{z})$ due to $\boldsymbol{f}_{nl}$ depends on x. Instead a technique called the *alternating frequency-time domain*(AFT) method is used. Here $\boldsymbol{b}$ is calculated through successive Fourier transformations as shown in the graph below.

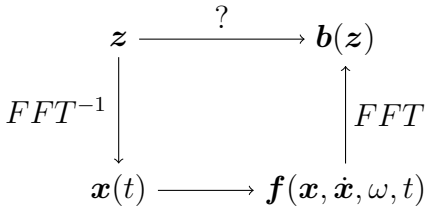

Figure 3.1.2: *Graphical representation of the alternating frequency-time domain (AFT) method*

$\boldsymbol{x}$ is calculated from the Fourier coefficients in $\boldsymbol{z}$, then the nonlinear (and external) forces $\boldsymbol{f}$ are evaluated in time domain and $\boldsymbol{b}$ is found as the Fourier coefficients of $\boldsymbol{f}$.

The Jacobian matrix is given by

$$\boldsymbol{H}_{\boldsymbol{z}} = \frac{\partial \boldsymbol{H}}{\partial \boldsymbol{z}} = \boldsymbol{A} - \frac{\partial \boldsymbol{b}}{\partial \boldsymbol{z}} \tag{3.1.30}$$

where the hard part is to compute $\boldsymbol{b}_{\boldsymbol{z}}$. The method for calculating the Jacobian matrix follows the AFT method as well. To do that, the inverse Fourier transform is rewritten as the linear operator $\Gamma(\omega)$

$$\begin{aligned}\boldsymbol{\Gamma}(\omega) = \Bigg[& \mathbb{I}_n \otimes \begin{bmatrix} 1/\sqrt{2} \\ 1/\sqrt{2} \\ \vdots \\ 1/\sqrt{2} \end{bmatrix} \quad \mathbb{I}_n \otimes \begin{bmatrix} \sin(\omega t_1) \\ \sin(\omega t_2) \\ \vdots \\ \sin(\omega t_{t_N}) \end{bmatrix} \quad \mathbb{I}_n \otimes \begin{bmatrix} \cos(\omega t_1) \\ \cos(\omega t_2) \\ \vdots \\ \cos(\omega t_{t_N}) \end{bmatrix} \quad \cdots \\ & \mathbb{I}_n \otimes \begin{bmatrix} \sin(N_H \omega t) \\ \sin(N_H \omega t_2) \\ \vdots \\ \sin(N_H \omega t_{t_N}) \end{bmatrix} \quad \mathbb{I}_n \otimes \begin{bmatrix} \cos(N_H \omega t) \\ \cos(N_H \omega t_2) \\ \vdots \\ \cos(N_H \omega t_{t_N}) \end{bmatrix} \Bigg]\end{aligned} \tag{3.1.31}$$

which is used on the concatenated time series

$$\begin{aligned}\tilde{\boldsymbol{x}} &= \begin{bmatrix} x_1(t_1) & \cdots & x_1(t_N) & \cdots & x_n(t_1) & \cdots & x_n(t_N) \end{bmatrix}^T \\ \tilde{\boldsymbol{f}} &= \begin{bmatrix} f_1(t_1) & \cdots & f_1(t_N) & \cdots & f_n(t_1) & \cdots & f_n(t_N) \end{bmatrix}^T\end{aligned} \tag{3.1.32}$$

Thus the inverse and direct Fourier transform are written

$$\tilde{\boldsymbol{x}} = \boldsymbol{\Gamma}(\omega)\boldsymbol{z}, \quad \boldsymbol{z} = (\boldsymbol{\Gamma}(\omega))^{+}\tilde{\boldsymbol{x}} \tag{3.1.33}$$

where $()^+$ is the Moore-Penrose pseduinverse which is needed since Γ is not square. (In implementing, one would use a least-square iterative solver instead of calculating the pseduinverse, since the former is faster. Both methods gives a solution which have a minimum norm in some sense.)

The Fourier coefficients of the external and nonlinear forces are then

$$\boldsymbol{b}(\boldsymbol{z}) = (\boldsymbol{\Gamma}(\omega))^+ \tilde{\boldsymbol{f}} \tag{3.1.34}$$

and the Jacobian is computed as

$$\boldsymbol{H}_z = \boldsymbol{A} - \frac{\partial \boldsymbol{b}}{\partial \boldsymbol{z}} = \boldsymbol{A} - \frac{\partial \boldsymbol{b}}{\partial \tilde{\boldsymbol{f}}} \frac{\partial \tilde{\boldsymbol{f}}}{\partial \tilde{\boldsymbol{x}}} \frac{\partial \tilde{\boldsymbol{x}}}{\partial \boldsymbol{z}} = \boldsymbol{A} - \boldsymbol{\Gamma}^+ \frac{\partial \tilde{\boldsymbol{f}}}{\partial \tilde{\boldsymbol{x}}} \boldsymbol{\Gamma} \tag{3.1.35}$$

It should be noted that the concatenated time series vectors $\tilde{\boldsymbol{x}}$ and $\tilde{\boldsymbol{f}}$ are newer used. They are only used in the derivation for the expression for the Jacobian. Only the Fourier operator $\boldsymbol{\Gamma}$ and extracted Fourier coefficients $\boldsymbol{x}$ are used.

Stability

Unlike the shooting method (or general time domain methods), the monodromy matrix is not readily available as a byproduct since there is no time integration. Instead for frequency methods, *Hills method* is used to approximate the Floquet exponents by solving a quadratic eigenvalue problem whose components are obtained as byproduct of the HB method.

Perturbing a periodic solution by an exponential decay

$$\boldsymbol{p}(t) = \boldsymbol{x}(t) + e^{\lambda t} \boldsymbol{s}(t) \tag{3.1.36}$$

and inserting this into the eom eq. (**??**) it is shown in appendix **??** that the quadratic eigenvalue problem is found as

$$\boldsymbol{\Delta}_2 \boldsymbol{\lambda}^2 + \boldsymbol{\Delta}_1 \boldsymbol{\lambda} + \boldsymbol{H}_z = \boldsymbol{0} \tag{3.1.37}$$

where $\boldsymbol{\Delta}$ are matrices describing the linear dynamics similar to $\boldsymbol{A}$ in eq. (**??**) and λ are Hills coefficients.

The quadratic eigenvalue problem is rewritten to a linear eigenvalue problem of double size

$$\boldsymbol{B}_1 - \gamma \boldsymbol{B}_2 = \boldsymbol{0} \tag{3.1.38}$$

where

$$\boldsymbol{B}_1 = \begin{bmatrix} \boldsymbol{\Delta} B_1 & \boldsymbol{H}_z \\ -\mathbb{I} & \boldsymbol{0} \end{bmatrix}, \quad \boldsymbol{B}_2 = -\begin{bmatrix} \boldsymbol{\Delta}_2 & \boldsymbol{0} \\ \boldsymbol{0} & \mathbb{I} \end{bmatrix} \tag{3.1.39}$$

The coefficients $\boldsymbol{\lambda}$ are found as the eigenvalues of the $(2N_H+1)2n \times (2N_H+1)2n$ matrix

$$\boldsymbol{B} = \boldsymbol{B}_2^{-1} \boldsymbol{B}_1 = \begin{bmatrix} -\boldsymbol{\Delta}_2^{-1} \boldsymbol{\Delta}_1 & -\boldsymbol{\Delta}_2^{-1} \boldsymbol{H}_z \\ \mathbb{I} & \boldsymbol{0} \end{bmatrix} \tag{3.1.40}$$

or from the generalised eigenvalueproblem eq. (**??**).

Only $2n$ eigenvalues approximate the Floquet exponents $\tilde{\boldsymbol{\lambda}}$, the rest are spurious. The real ones are the $2n$ values with smallest imaginary magnitude.

The diagonal matrix

$$\tilde{\boldsymbol{B}} = \begin{bmatrix} \tilde{\lambda}_1 & & \\ & \ddots & \\ & & \tilde{\lambda}_{2n} \end{bmatrix} \tag{3.1.41}$$

gathers the Floquet exponents identified from the $(2_{N_H} + 1)2n$ Hill's coefficients. Besides stability, they are used for detecting bifurcations in section **??**.

Example

Figure **??** shows the periodic of the coupled duffing Duffing system. Although the excitation is pure sine, the response contains multiple harmonics due to nonlinearity. The normalized harmonic components are found as

$$\begin{aligned} \sigma_i &= \frac{\phi_i}{\sum_{k=0}^{N_H} \phi_i}, \quad (i = 0, \cdots, N_H) \\ \phi_0 &= \frac{c_0^x}{\sqrt{2}}, \quad \phi_i = \sqrt{(s_i^x) + (c_i^x)^2} \end{aligned} \tag{3.1.42}$$

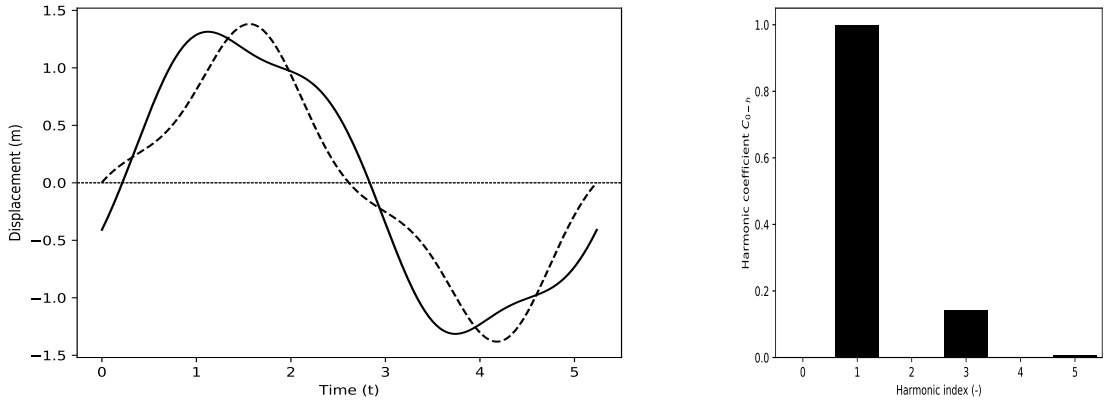

(a) **(b)**

Figure 3.1.3: *Periodic solution of the coupled Duffing system for $f = 2$, $\omega = 1.2$ and $N_H = 5$. (a): Time series; (b): Normalized harmonic components of x_1.*

Summary

Periodic solutions of nonlinear structures can be computed with time-domain(shooting method) and frequency-domain(harmonic balance) methods. The main difference is in the implementation complexity, computional complexity and accuracy. Both methods can be used together with continuation and are natural integrated with stability analysis.

Summarising the shooting method

Pro	Cons
• Accurate	• Many time integrations
• Higher harmonics represented	• Slow for larger systems

If the shooting method should be used for damped and forced motion, only the state space formulation have to be changed. See appendix **??** for the few changes.

Summarising the harmonic balance method

Pro	Cons
• Fast	• Less accurate
• Harmonic coefficients available	• High number of harmonic might be necessary. Need to check the contribution from last harmonics to ensure enough is included.
• Can be used for filtering	

Stability of a periodic solution can be assessed through their Floquet multipliers or exponents. When the Shooting method is used, they are found from the monodromy matrix. When Harmonic balance (HB) is used, they are found from Hills matrix.

3.2 Continuation

When the periodic solution is found, finding the successively periodic solutions is done by continuation.

As with finding periodic solutions, there exist multiple schemes to do continuation. A general continuation is formulated as $F(x) = 0, \quad F : \mathbb{R}^{m+1} \to \mathbb{R}^m$, ie. here the structure is $\boldsymbol{z} \in \mathbb{R}^m$, $\omega \in \mathbb{R}^1$ and F the algebraic problem for which a solution is sought.

The most simple continuation method, where ω is used as independent parameter and uniformly increased at each step fails at turning points. Instead most continuation methods uses a length-wise curve parameter and a predictor-corrector model. Starting from a known solution $\boldsymbol{y}_j = [\boldsymbol{z}_{p0,(j)}, \omega_{(j)}]^T$ the next periodic solution $\boldsymbol{y}_{j+1}$ is found as

- Tangent prediction, $\boldsymbol{y}^1_{(j+1)} = y_{(j)} + s\boldsymbol{t}_{(i)}$, where s is the step size and $\boldsymbol{t}$ the tangent.
- Newton-like corrections - The type determines the continuation method.
- Adaptive step control. Here a simple model using the convergence of the Newton iterations is used: $s = \frac{it_{opt}}{it_{NR}} s$, ie. the step is updated based on the defined optimal number of iterations versus the actual used number of iteration

The two methods used in this project are the pseudo-archlength continuation and the Moore-Penrose continuation. The main difference is computional complexity. With pseudo-archlength, each time a new point is found on the curve, the tangent vector have to be computed anew. With the Moore-penrose corrector, the tangent vector is also corrected and we save the explicit calculation of the tangent at each new point.

The aim is to show that is no harder to use the Moore-penrose corrector. Formal descriptions are found in [6]

Procedure

The tangent at a solution point $\boldsymbol{y}_i$ is

$$\begin{bmatrix} \boldsymbol{J}(\boldsymbol{y}_{(i)}) \\ \boldsymbol{t}^T_{(i-1)} \end{bmatrix} \boldsymbol{t}_i = \begin{bmatrix} \boldsymbol{0} \\ 1 \end{bmatrix} \tag{3.2.1}$$

where

$$\boldsymbol{J}(\boldsymbol{y}_{(i)}) = \begin{bmatrix} \boldsymbol{H}_{\boldsymbol{z}}(\boldsymbol{y}_{(i)}) & \boldsymbol{H}_{\omega}(\boldsymbol{y}_{(i)}) \end{bmatrix} \tag{3.2.2}$$

The last row in eq. (**??**) prevents the continuation from turning back, $\boldsymbol{t}_{(i)}\boldsymbol{t}_{(i+1)} = 1$. For the first tangent calculation it is replaced by a row of ones, which impose the length of the tangent to 1; later predictions $\boldsymbol{t}_{(i+1)}$ must be normalized. The prediction is then

$$\boldsymbol{y}^{(1)}_{(i+1)} = \boldsymbol{y}_{(i+1)} + s\boldsymbol{t}_i \tag{3.2.3}$$

The corrections Pseudo-archlength and Moore-penrose are used with the shooting method and harmonic balance, respectively. Convergence is achieved when

$$\frac{\|\boldsymbol{h}\|}{\|\boldsymbol{z}\|} < tol \tag{3.2.4}$$

Shooting methods

For the pseudo-archlength corrections, a solution is sought in the perpendicular direction of the prediction. The corrections are given by

$$\boldsymbol{y}^{(j+1)} = \boldsymbol{y}^{(j+1)} + \Delta\boldsymbol{y} = \boldsymbol{y}^{(j+1)} - \boldsymbol{G}_{\boldsymbol{y}}^{-1}\boldsymbol{G} \tag{3.2.5}$$

where the prediction subscripts have been omitted. We have

$$\boldsymbol{G}(\boldsymbol{y}) = \begin{bmatrix} \boldsymbol{H}(\boldsymbol{y}) \\ \boldsymbol{0} \end{bmatrix}, \quad \boldsymbol{G}_{\boldsymbol{y}}(\boldsymbol{y}) = \begin{bmatrix} \boldsymbol{J}(\boldsymbol{y}) \\ \boldsymbol{t}^T \end{bmatrix} \tag{3.2.6}$$

where correction superscripts have been omitted. After convergence to a solution, the tangent is calculated and the algorithm continues.

Harmonic balance

For the Harmonic balance method the nearest solution to the prediction is sought. This is done by updating the tangent direction at each corrector iteration. But first $\boldsymbol{h}_\omega$ in eq. (**??**) is given by

$$\boldsymbol{h}_\omega = \frac{\partial \boldsymbol{A}}{\partial \omega}\boldsymbol{z} \tag{3.2.7}$$

Using a optimisation variable $\boldsymbol{v}$, initialised as the prediction tangent $\boldsymbol{v}^{(1)} = \boldsymbol{t}_{(i)}$, the Moore-penrose corrections are given by

$$\begin{aligned} \boldsymbol{y}^{(j+1)} &= \boldsymbol{y}^{(j+1)} + \Delta\boldsymbol{y} = \boldsymbol{y}^{(j+1)} - \boldsymbol{G}_{\boldsymbol{y}}^{-1}\boldsymbol{G} \\ \boldsymbol{v}^{(j+1)} &= \boldsymbol{v}^{(j+1)} + \Delta\boldsymbol{y} = \boldsymbol{v}^{(j+1)} - \boldsymbol{G}_{\boldsymbol{y}}^{-1}\boldsymbol{R} \end{aligned} \tag{3.2.8}$$

where the prediction subscripts have been omitted. We have

$$\begin{aligned} \boldsymbol{G}(\boldsymbol{y},\boldsymbol{v}) = \begin{bmatrix} \boldsymbol{H}(\boldsymbol{y}) \\ \boldsymbol{0} \end{bmatrix}, \quad \boldsymbol{G}_{\boldsymbol{y}}(\boldsymbol{y},\boldsymbol{v}) &= \begin{bmatrix} \boldsymbol{J}(\boldsymbol{y}) \\ \boldsymbol{v}^T \end{bmatrix} \\ \boldsymbol{R}(\boldsymbol{y},\boldsymbol{v}) &= \begin{bmatrix} \boldsymbol{J}(\boldsymbol{y})\boldsymbol{v} \\ \boldsymbol{0} \end{bmatrix} \end{aligned} \tag{3.2.9}$$

where correction superscripts have been omitted.

When convergence is reached the tangent is calculated as the normalized correction of $\boldsymbol{v}$, $\boldsymbol{t}_{(j+1)} = \frac{\boldsymbol{v}}{\|\boldsymbol{v}\|}$.

During the corrections eq. (**??**-**??**) $\boldsymbol{H}_{\boldsymbol{z}}$ is calculated, making stability analysis with Hills method cheap after each solution is obtained.

Example

Figure **??** shows the NRFC for the coupled duffing using five harmonic terms. That is enough to capture the harmonic components, as seen in figure **??**. If a lower number of harmonic were included - only one and three terms would be relevant since even harmonics are zero; it would required an even nonlinearity to generate even harmonics - the superharmonic resonances at lower frequencies will not be captured. See appendix **??** where NRFCs are shown for different HB and continuation parameters.

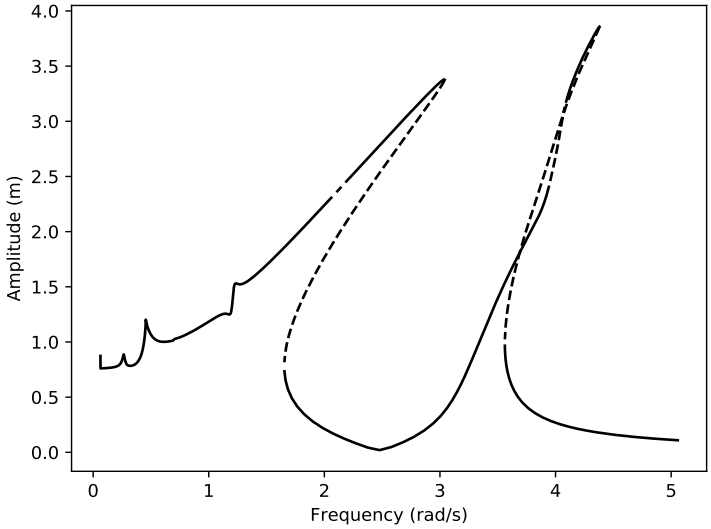

Figure 3.2.1: *NRFC of the coupled duffing system for x_1 with $f = 2N$. Unstable branches are indicated by $- - -$. $N_H = 5, N = 512$*

Summary

Figure **??** show the continuation procedure, regardless of the the correction method. There is not much difference if implementation complexity, but the Moore-penrose corrections saves on computional complexity. The Pseudo-arclength method can be seen as a Moore-Penrose method for which the correction direction is not updated.

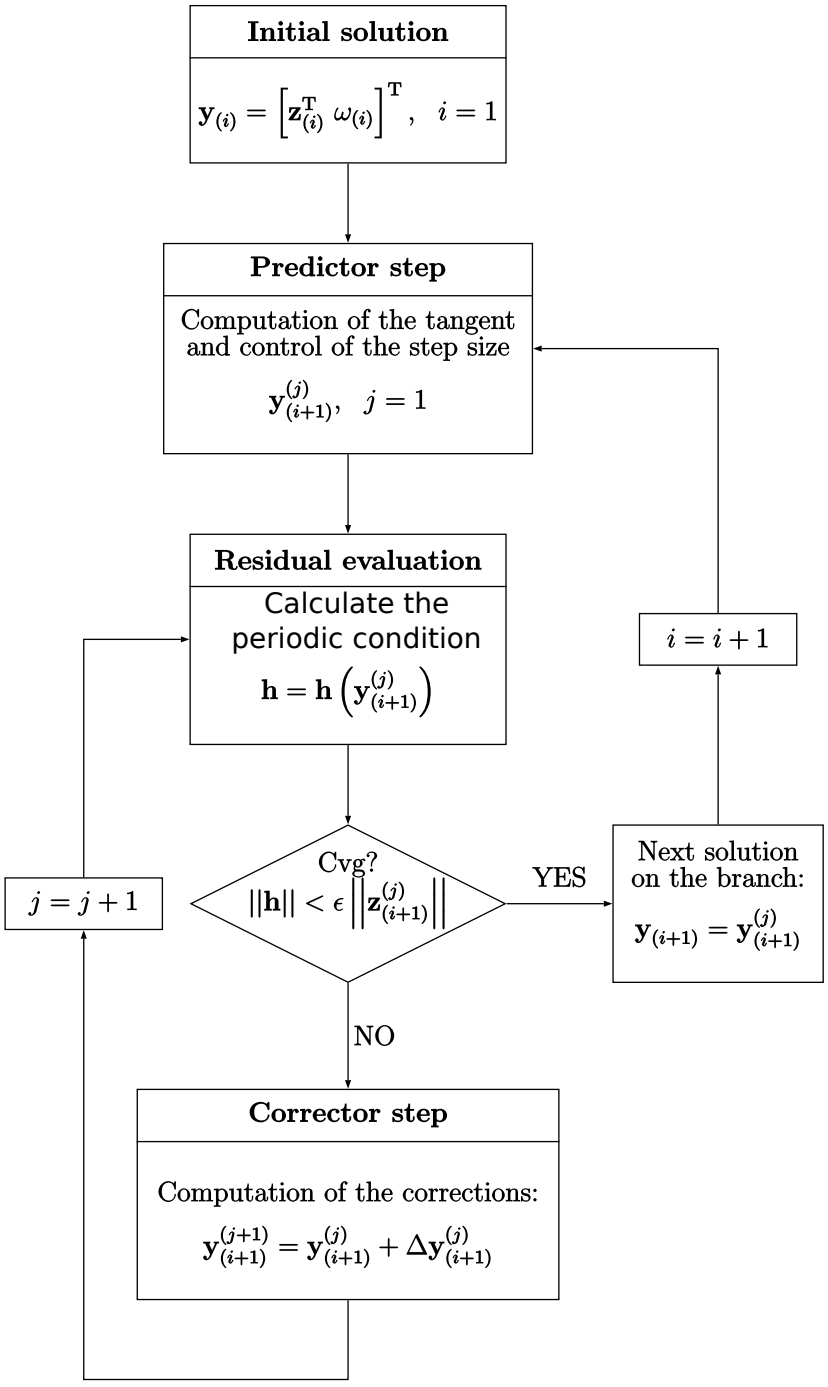

Figure 3.2.2: *Algorithm for Predictor-Corrector continuation of a periodic solution. For Moore-penrose the successive tangents are simply calculated as a normalization.*

3.3 Bifurcations

When stability of periodic solutions changes, it occurs at points called *bifurcation points*. At bifurcation points, the solution changes qualitatively, but knowledge of the bifurcation type allows to predict the behaviour. The type of bifurcation is related to how the Floquet multipliers changes at said point, and the mechanism for loss of stability for the three most common types are shown in figure **??**

Bifurcations exist for multiple dimensions, but only codimension-1 bifurcations are treated as only one parameter varies along the branch (ie. the forcing frequency ω). Bifurcations are a feature of nonlinear systems. Further description is found in [14] or dedicated bifurcation textbooks like [**kuznetsov2013**]. Floquet multipliers σ_i and Floquet exponents λ_i are related as (as restated from eq. (**??**))

$$\sigma_i = e^{\lambda_i T} \tag{3.3.1}$$

Singulare Bifurcation Point

At Singulare bifurcation point the system undergoes amplitude jumps (fold bifurcation) or branching (branch point bifurcation), see below. A singular point is detected when a Floquet multiplier leaves the unit circle along the real axis through +1 or, equivalently, when a Floquet exponent crosses the imaginary axis through 0, see Figs **??**(a,b)

The term singular refers to that at this point, the Jacobian matrix $\boldsymbol{h_z}$ is singular: if $\boldsymbol{h_z}$ is singular then the monodromy matrix of the Shooting method or $\boldsymbol{B}$ of HB, eq (**??**), is also singular and at least one Floquet exponent is 0 (or a Floquet multiplier crosses the unit circle through +1)

Two types of singular bifurcations exist:

- *Fold bifurcation* (also denoted Saddle node, Limit point or Turning point):
  The branch comes from one side and turns back, ie. the parameter(ω) increases and then decreases or decreases and then increases. Thus fold bifurcation indicates that there exist two solutions in its vicinity. It determines the upper or lower region of a bistable region and is often present in the vicinity of resonance peaks. This is the cause of amplitude jumps seen as response to stepped- or swept-sine excitation.

- *Bifurcation point (BP)*:
  Two branches are connected. The two branches either meet and exchange stability (transcritical bifurcation), or one branch loses stability and a stable branch emanates from the point (pitchfork bifurcation).

Fold bifurcations satisfies

$$\boldsymbol{h}_\omega \notin \text{range}(\boldsymbol{h_z}) \tag{3.3.2}$$

whereas for BPs

$$\boldsymbol{h}_\omega \in \text{range}(\boldsymbol{h_z}) \tag{3.3.3}$$

It follows that fold and BPs can be found, and distinguished, by calculating the rank of the extended Jacobian $\boldsymbol{J} = [\boldsymbol{h_z}|\boldsymbol{h}_\omega]$ and $\boldsymbol{h_z}$. If the rank of $\boldsymbol{J}$ is equal to $\boldsymbol{h_z}$(and $\boldsymbol{h_z}$ is singular), then it is a BP otherwise fold(and $\boldsymbol{J}$ have full rank)

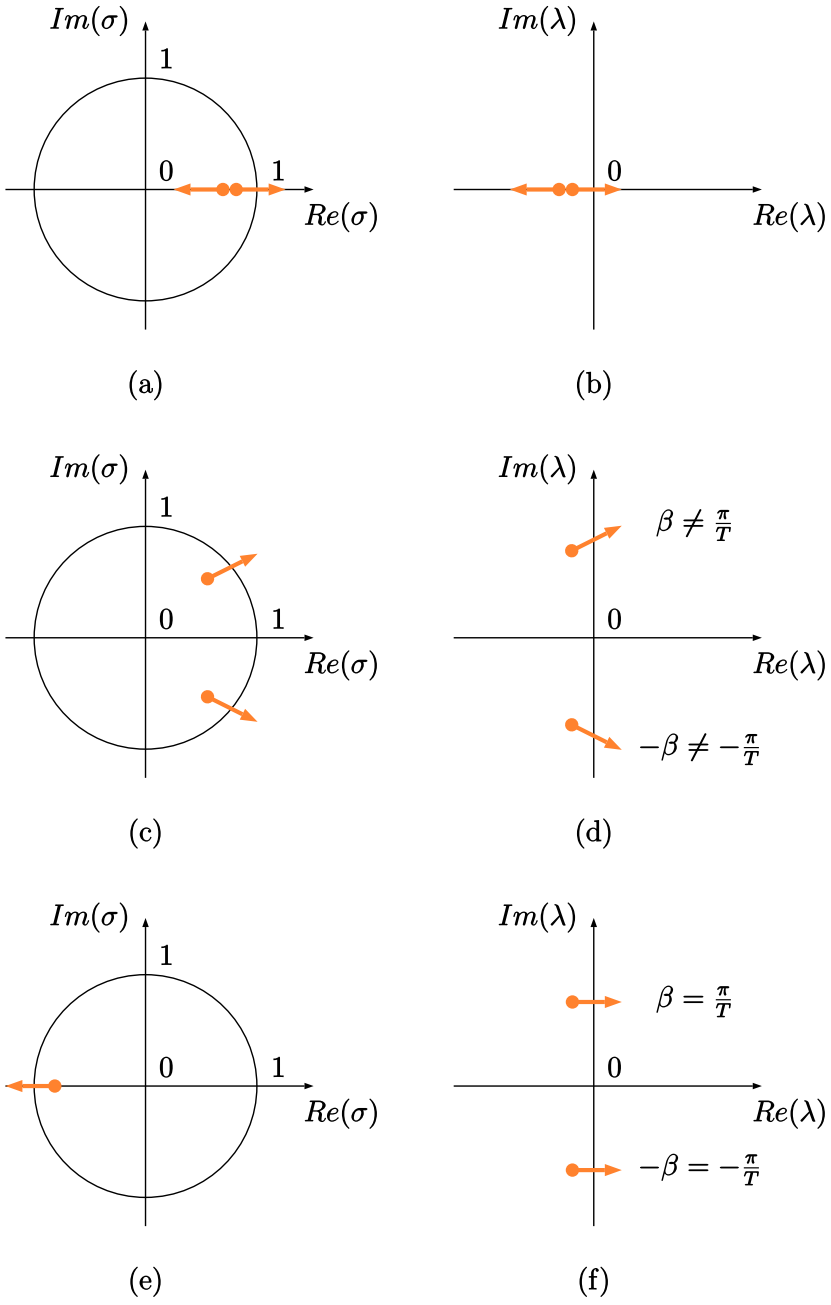

Figure 3.3.1: *Mechanisms for the loss of stability of a periodic solution, illustrated with Floquet multipliers (left column) and Floquet exponents (right column).* ***First row****: singular point;* ***Second row****: Neimark-Sacker bifurcation;* ***third row****: period doubling bifurcation. Reproduced from [3]*

If a BP is found, some branch switching mechanism should be used in the continuation in order to switch branch. If no switching mechanism is used, the continuation most likely continues on the same branch through the BP. The new branch is found by calculating the two tangent directions at the BP; thus some adoption of the predictor method is needed.

Neimark-Sacker bifurcation

A Neimark-Sacker bifurcation (NS) (also called Hopf- or torus bifurcation) is detected when a pair of Floquet multipliers leaves the unit circle as complex conjugates or, equivalently, when a pair of Floquet exponent crosses the imaginary axis as complex conjugates through any value but $\pm\frac{i\pi}{T}$ where T is the period of oscillation, see Figs **??**(c,d)

At NS a new type of oscillations emerges. These are called Quasiperiodic oscillations (QP) and despite the name they are not periodic. QPs contain the forcing frequency ω (forcing), and at least another frequency ω_2(envelope). The two frequencies are incommensurate, ie. $\frac{\omega}{\omega_2}$ is irrational. It should not confused with linear beating, where the forcing frequency is close to the eigenfrequency ω_0, ie. $|\omega_0 - \omega|$ is small.

The imaginary part of the Floquet exponents that cross the imaginary axis, β, approximates the envelope pulsation ω_2 of the BP in the vicinity of the bifurcation, see Fig. **??**(d)

Period doubling bifurcation

A Period doubling bifurcation (PD) (also called flip bifurcation) is detected when a pair of Floquet multipliers leaves the unit circle along the real axis through -1 or, equivalently, when a pair of Floquet exponent crosses the imaginary axis as complex conjugates through $\pm\frac{i\pi}{T}$, see Figs. **??**(e,f).

At PDs a new branch of solution appears. The new branch have stable periodic solutions with a doubled period. When they appear in cascade, PD can lead to chaos.

3.4 Detecting bifurcations

To detect bifurcations during the continuation procedure, *test functions* ϕ are monitored. When they change sign, a bifurcation is detected. Each type of bifurcation have their own test function

Singulare Bifurcation Point

As stated, fold and BP are characterised by rank deficiency of the Jacobian matrix $\boldsymbol{h_z}$. Thus a test function could be

$$\phi_{F,BP} = \det \boldsymbol{h_z} \tag{3.4.1}$$

a computationally cheaper detection could be based on the monodromy or Hills matrix, since this is already available

$$\phi_{F,BP} = \det \tilde{\boldsymbol{B}} \tag{3.4.2}$$

To distinguish between fold and BP a dedicated test function is

$$\phi_{BP} = \det \begin{pmatrix} \boldsymbol{h_z} & \boldsymbol{h}_\omega \\ \boldsymbol{t}^T & \end{pmatrix} \tag{3.4.3}$$

For detection fold bifurcation alone, a computationally cheaper way is to use the geometric folding of the branch, ie. detect when the ω component of the tangent prediction $\boldsymbol{t}$ changes sign,

$$\phi_F = t_\omega \tag{3.4.4}$$

Neimark-Sacker and period doubling bifurcation

Bifurcations for which a pair of Floquet exponents crosses the imaginary axis as complex conjugates, i.e. NS and PD bifurcations, can be detected using the theory of the bialternate product of a matrix. The bialternate product $\boldsymbol{P}_\odot$ of a $m \times m$ matrix $\boldsymbol{P}$ is

$$\boldsymbol{P}_\odot = 2\boldsymbol{P} \odot I_m \tag{3.4.5}$$

with dimensions $m(m-1)/2$, is singular when two of its eigenvalues, $\mu 1$ and $\mu 2$, verify:

$$\mu_1 + \mu_2 = 0 \tag{3.4.6}$$

which is true for two purely imaginary- or real conjugate. Thus the test function is

$$\phi_{NS,PD} = \det\left(\tilde{\boldsymbol{B}}_\odot\right) \tag{3.4.7}$$

When the test function is zero, the Floquet exponents are checked. Two real conjugates are associated with a neutral saddle point, which is not considered a bifurcation and is ignored.

Since $\tilde{\boldsymbol{B}}$ is diagonal, the bialternate product is also diagonal.

Bordering technique

Calculating the determinants needed for BP, NS and PD detection for large scale structures might not be numerical stable. Instead the *bordering technique* might be used, where the calculation of the determinant of $\boldsymbol{G}$ is replaced with calculation of a scalar function g which vanishes at the same time as the determinant [**kuznetsov2013**]

$$\begin{bmatrix} \boldsymbol{G} & \boldsymbol{p} \\ \boldsymbol{q}^* & 0 \end{bmatrix} \begin{bmatrix} \boldsymbol{w} \\ q \end{bmatrix} = \begin{bmatrix} \boldsymbol{0} \\ 1 \end{bmatrix} \tag{3.4.8}$$

where vectors $\boldsymbol{p}$ and $\boldsymbol{q}$ can be arbitrarily chosen as long as they ensure nonsingularity of the system. This means they must be adapted along the branch to ensure good conditioning of the bordered matrix.

g is related to $\boldsymbol{G}$ by Cramer's rule

$$g = \frac{\det \begin{pmatrix} \boldsymbol{G} & 0 \\ \boldsymbol{q}^* & 1 \end{pmatrix}}{\det \begin{pmatrix} \boldsymbol{G} & \boldsymbol{p} \\ \boldsymbol{q}^* & 0 \end{pmatrix}} = \frac{\det(\boldsymbol{G})}{\det \begin{pmatrix} \boldsymbol{G} & \boldsymbol{p} \\ \boldsymbol{q}^* & 0 \end{pmatrix}} \tag{3.4.9}$$

Example

The bifurcations for the coupled duffing system is shown in figure **??**. Fold, BP and NS bifurcations are found along the branch. As expected fold bifurcations are found close to the two resonance peaks. In fig. **??**(b) a branch of periodic solutions emerges from a BP bifurcation. In fig **??**(c) QP oscillations appears after a NS bifurcation.

along

Figure 3.4.1: *Bifurcation analysis of the coupled Duffing system at x_1 for $f = 2N$.* ***(a)*** *Stable and unstable solutions are represented with solid and dashed lines. Fold, BP and NS bifurcations are represented with orange circle, red square and blue triangle markers, respectively. Insets display the evolution of Floquet exponents.* ***(b)*** *Close-up of the NRFC in the vicinity of the BPs and the emanating branch.* ***(c)*** *QP oscillations for a forcing frequency of $\omega = 4$ rad/s.*

The evaluation of test functions for BP bifurcations along the branch is shown in fig. **??**. In fig **??**(c) it seen that the test function based on the determinant become very large close to singular points whereas the bordering technique produce numerical stable values.

along

Figure 3.4.2: *Test functions for BP detection.* ***(a)*** *NRFC and BP bifurcations;* ***(b)*** *test function based on the bordering technique;* ***(c)*** *test function based on the determinant. It is noted that the determinant gets higher than 10^{28} and the machine precision for a double precision 64 bit number is $\epsilon = 2^{-52} \sim 10^{-}16$, which means that the maximum spacing between two (normalised) numbers can be at max $2\epsilon|x|$ in order to be represented correct.*

Summary

Bifurcation analysis can help understand nonlinear phenomena such as amplitude jumps, quasiperiodic oscillations and period doubling. They are found during continuation by using test functions, where a resume is shown in fig **??** for Hills method.

1. Detection of *fold bifurcation*:

$$\phi_F = t_w$$

2. Detection of *bifurcation point* (BP):

$$\phi_{BP} = g_{bp}$$

from the bordering system in eq. **??** with

$$\boldsymbol{G}_{BP} \begin{bmatrix} \boldsymbol{h_z} & \boldsymbol{h}_\omega \\ & \boldsymbol{t}^T \end{bmatrix}$$

3. Detection of *Neimark-Sacker* (NS) and *period doubling* (PD) bifurcations:

$$\phi_{NS,PD} = g_{NS,PD}$$

from the bordering system in eq. **??** with $\boldsymbol{G}_{NS,PD} = \tilde{\boldsymbol{B}}_\odot$. When $\phi_{NS,PD} = 0$, matrix $\tilde{\boldsymbol{B}}$ has μ_1 and μ_2 among its eigenvalues, with

$$\mu_1 + \mu_2 = 0$$

- If $\mu_{1,2} = \pm i\beta$ with $\beta \neq \pi/T$, a NS bifurcation is detected.
- If $\mu_{1,2} = \pm i\beta$ with $\beta = \pi/T$, a PD bifurcation is detected.
- If $\mu_{1,2} = \pm\beta$ with $\beta \in \mathbb{R}$, a neutral saddle point is detected.

Figure 3.4.3: *Test functions for detection of codimensional-1 bifurcation of NFRCs*

3.5 Nonlinear normal modes

The (numerical) calculations of NNMs were introduced in Peeters et al. [27], using a shooting method and pseudo-archlength continuation technique.

The shooting method requires substantial computational effort for larger FEM structures. A method based on harmonic balance (HB) and continuation was recently introduced in the review by Renson [28], which, among several benefits, reduces the computational burden. The HB method for NNMs originated from Detroux, Renson, and Kerschen [4]. A method for calculating NNMs for nonconservative systems, mentioned in the review and originating from Renson [29], will not be studied in this thesis.

This is because for simple (and weekly) damping mechanism, the damped dynamics can often be interpreted based on the topological structure and bifurcation of the NNMs of the underlying Hamiltonian(conservative) system, [28, sec. 4]

A so far very incomplete description

Modal features are often used to examine vibrating structures, and for linear structures, the theory and practice is well established.

The chapter introduce the concept of nonlinear normal modes (NNM), stating with a recap of linear normal modes (LNM). A more in-depth investigation and history of NNMs can be found in [15] and the monograph [33, chap 2.].

Linear normal modes

Linear normal modes is a central part of linear vibration theory.

They have a clear physical interpretation: when a system vibrates at a mode, all parts of the system moves sinusoidal with a fixed phase. Further the mathematical properties of LNMs allow for decoupling of the governing equations, i.e. a linear system vibrates as if it were made of independent oscillators governed by the eigensolution. The invariance and modal superposition comes from this decoupling:

- Invariance: If the motion is initiated on one specific LNM, the remaining LNMs remain quiescent for all time
- Modal superposition: Free and forced vibrations can conveniently be expressed as linear combinations of individual LNM motions.

The theory and application of LNM is extensive and mature, including model reduction (substructuring techniques [2]), experimental modal analysis [9], finite element model updating (and validating)[10] and structural health monitoring [7].

For nonlinear system, attempts to apply linear analysis results at best in a suboptimal design. NMM is an attempt to generalize to concept of normal modes to nonlinear systems. NMM was first defined by Lyaponov, but today two definitions of NMMs are generally used:

Targeting a nonlinear extension of LNMs, [30] gave a definition of NNMs, for an undamped system, as a *v*ibration in unison of the system, i.e. a synchronous periodic oscillation. This requires that all points of the system reach their extreme values and pass through zero simultaneous, allowing all displacements to be expressed in terms of

a single reference displacement. From this it follows that in the configuration space of the system, the NNM oscillation is represented by either a straight modal line (similar NNM) or a modal curve (non-similar NNM).

Similar NNMs are analogous to linear normal modes, in the sense that their modal lines do not depend on the energy of the free oscillation and space-time separation of the governing equations of motion can still be performed; however this type of NNMs is only realized when special symmetries occur, and are not typical (generic) in nonlinear systems. More generic are non-similar NNMs, whose modal curves do depend on energy; this energy dependence prevents the direct separation of space and time in the governing equations of motion by means of non-similar NNMs, which complicates their analytical computation.

Rosenbergs definition does not allow for internal resonance or damping. The latter was addressed by [31], who introduced the concept of *d*amped NNM invariant manifold to account for the fact that the free oscillation of a damped nonlinear system is a non-synchronous, decaying motion. Nothing more will be said about Shaws definition here, instead the reader can refer to [29] for a numerical implementation of this definition.

To account for internal resonance, i.e. some coordinates may vibrate faster than others and the system no longer vibrates in unison, [15] relaxed Rosenbergs definition to *(*not necessarily synchronous) time-periodic oscillation of a conservative system and is the definition used in this thesis.

Finally, with the present definition of NNMs, they have the following properties related to nonlinear systems:

- **F**requency-energy dependence
  One property of nonlinear systems is the frequency-energy dependence of their oscillations, e.g., through hardening or softening behaviors, and the FRF is no longer invariant. The evolution of NNMs along their backbone accounts for this dependence, as illustrated in Section **T**ODO. In some cases, the evolution of the modal properties results in the localization phenomenon, where vibration energy gets localized in a specific part of the structure.

- **I**nternal resonances
  During a general motion of the system, NNMs may interact. In the presence of these interactions, NNMs with well-separated fundamental frequencies can exchange energy.

  To expand a bit: At low energies these modes may possess incommensurate linearized natural frequencies so they do not satisfy internal resonance conditions. Due to the energy dependence of their frequencies, however, at higher energies the same NNMs may become internally resonant, as their energy-dependent frequencies may become commensurate resulting in strong nonlinear modal interactions

- **R**elations with forced responses
  For structures with low damping, the NNM backbone traces the locus of the resonance peaks.

They might also provide insight into when linear analysis can be used and not.

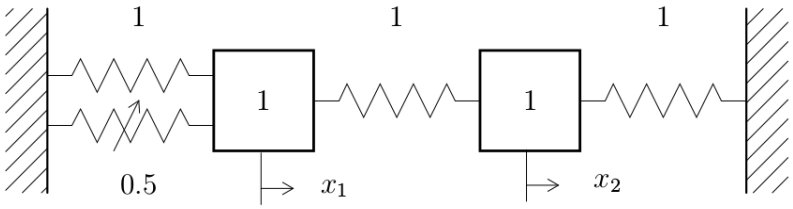

Figure 3.5.1: *Schematic representation of the 2DOF system*

As an example, consider the nonlinear 2DOF mass and spring system shown in figure **??**.

The equations of motion (EOM) are given by

$$\begin{aligned} \ddot{x}_1 + (2x_1 - x_2) + 0.5x_1^3 &= 0 \\ \ddot{x}_2 + (2x_2 - x_2) &= 0 \end{aligned} \tag{3.5.1}$$

Note that this system is not symmetric so it possess only non-similar NNMs.

The underlaying linear system is given by

$$\begin{aligned} \ddot{x}_1 + (2x_1 - x_2) &= 0 \\ \ddot{x}_2 + (2x_2 - x_2) &= 0 \end{aligned} \tag{3.5.2}$$

The initial condition that excites the two linear modes of system (**??**) is found from the eigensolution, i.e. the two eigenvectors.

Figure **??** and **??** shows the time series and configuration plane for in-phase and out-of-phase NNMs for the nonlinear system. The system vibrates in unison, even though higher harmonics are present as seen by the curved modal lines in the configuration plot.

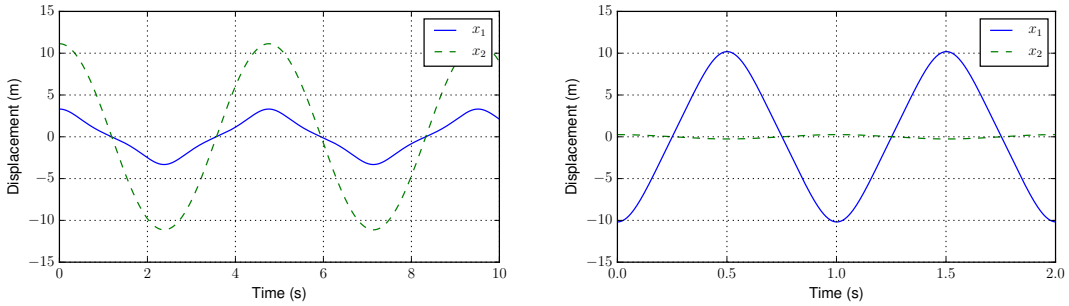

Figure 3.5.2: *Time series of system (**??**). Left plot: in-phase NNM,* $[x_1(0), x_2(0), \dot{x}_1(0), \dot{x}_2(0)] = [3.319, 11.134, 0, 0]$*; Right plot: out-of-phase NNM,* $[x_1(0), x_2(0), \dot{x}_1(0), \dot{x}_2(0)] = [-10.188, 0.262, 0, 0]$.

Figure **??** shows internal 3:1 resonance. The motion is still periodic, but not unison.

Similar NNM, an example

An example of similar NNMs are given in [32]. Given the symmetric system

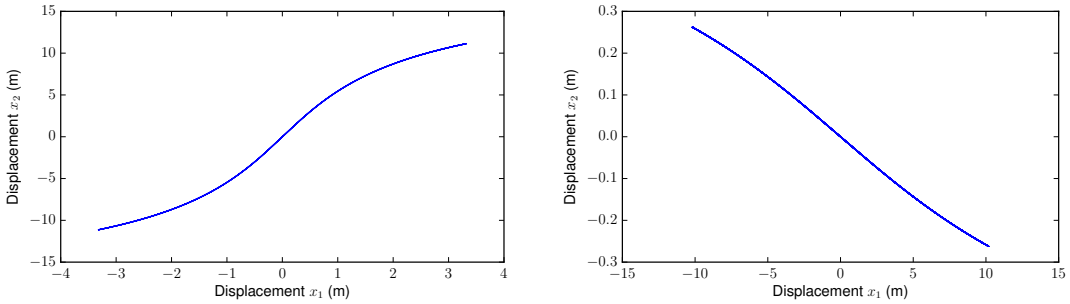

Figure 3.5.3: *NNM motion of system (??) in configuration space. Left plot: in-phase NNM; Right plot: of-phase NNM.*

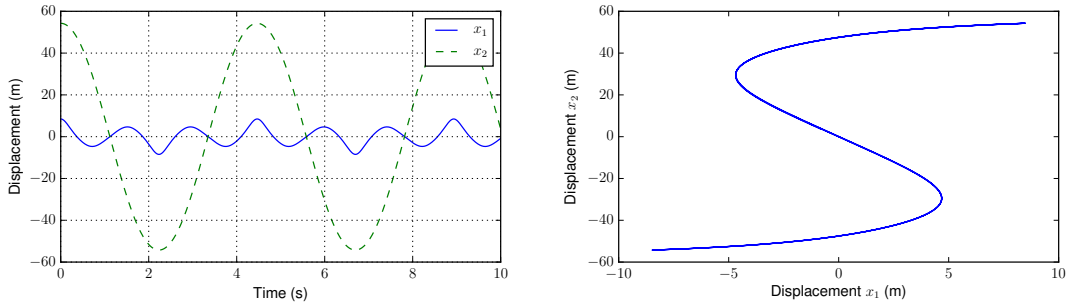

Figure 3.5.4: *Internally resonant NNM of system (??) (3:1 resonance);* $[x_1(0), x_2(0), \dot{x}_1(0), \dot{x}_2(0)] = [8.476, 54.263, 0, 0]$*; Left plot: time series; Right plot: configuration space*

$$\begin{aligned} \ddot{x}_1 + k_3(x_1 - x_2)^3 + x_1 + x_1^3 &= 0 \\ \ddot{x}_2 - k_3(x_2 - x_2)^3 + x_2 + x_2^3 &= 0 \end{aligned} \tag{3.5.3}$$

where k_3 is the strength of the nonlinear coupling. This system possesses only similar NNMs (due to the symmetry), which are found by imposing the functional relationship

$$x_2 = cx_1 \tag{3.5.4}$$

where $c \in \mathrm{Re}$ is a real modal constant. Substituting (??) into (??) to get a algebraic equation satisfied by the modal constant

$$k_3(1+c)(c-1)^3 = c(1-c^2) \tag{3.5.5}$$

From figure ?? it is seen that the system always possesses the NNMs $x_2 = \pm x_1$ regardless of the coupling strength. This correspond to the in-phase and out-of-phase similar NNMs respectively and can be regarded as as a continuation of the two normal modes of the corresponding linear system.

However at $k_3 = 1/4$, the out-of-phase NNM bifurcates. The bifurcating NNMs are out-of-phase, time-periodic motions of system and becomes strongly localized as $k_3 \to 0$, i.e. one node vibrates strongly while the other stands still. This shows another concept of NNM which differs from LNM: NNMs of a dynamical system may exceed

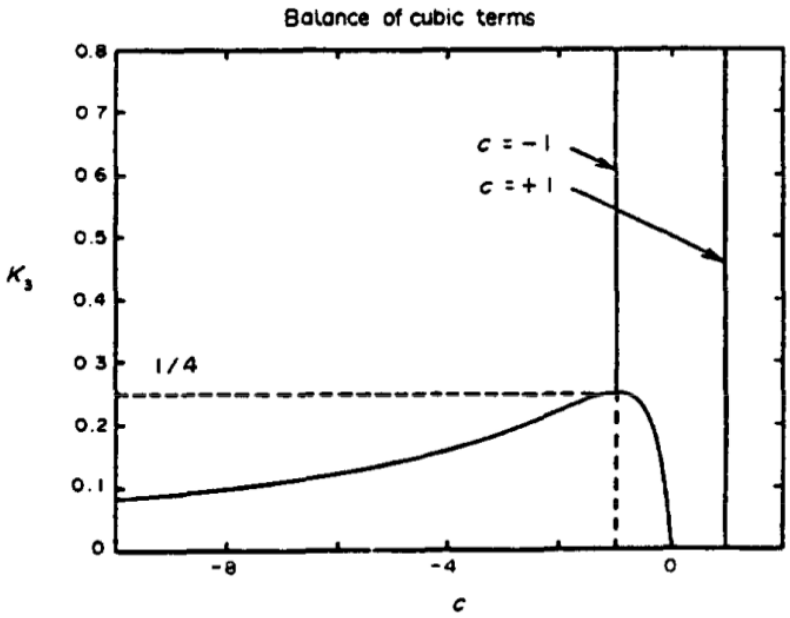

Figure 3.5.5: *Pichfork bifurcation of NMMs. (—) stable mode, (- - -) unstable mode. From [32]*

in number its degrees of freedom. Additionally, NNM bifurcations may result in mode instability.

Figure **??** shows the time series for out-of-phase NNMs for (**??**), and figure **??** shows the corresponding configuration space. For the bifurcated NNM, localization is seen. The system still vibrates with a single harmonic in unison, as seen by the straight line in configuration space and the time series.

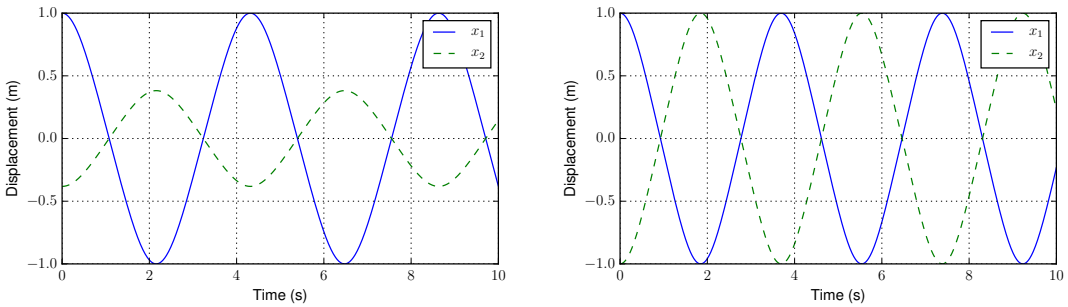

Figure 3.5.6: *Time series of system* (**??**). *Left plot: out-of-phase NNM,* $k_3 = 0.2$, $[x_1(0), x_2(0), \dot{x}_1(0), \dot{x}_2(0)] = [1, -1, 0, 0]$*; Right plot: out-of-phase NNM,* $k_3 = 0.2$, $[x_1(0), x_2(0), \dot{x}_1(0), \dot{x}_2(0)] = [1, -0.3820, 0, 0]$.

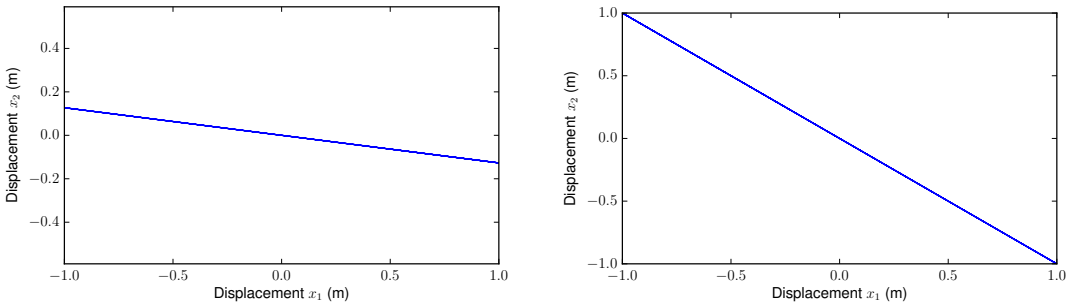

Figure 3.5.7: *NNM motion of system* (**??**) *in configuration space. Left plot: out-phase NNM; Right plot: out-of-phase NNM.*

Chapter 4

Signal treatment

Signal treatment and excitation type affects how the nonlinearity is seen in the measured signal. This chapter treats the types of excitation and treatments that is applicable for nonlinear dynamics.

4.1 Types of excitation

Different types of excitation gives different response for nonlinear structures, with certain types being superior for detecting and characterizing and others smooths out the nonlinearities. For a more in-depth treatment see [11].

- **s**teady state sine excitation:
  Generally *s*teady state sine excitation (or *s*tepped sine), gives the most distinctive nonlinear effects. All the input energy is contained in the frequency of excitation. Noise can be removed from the signal by numerical filtering and integration, giving a good signal-to-noise ratio (SNR) and thus well defined FRFs with clear nonlinear distortions.

  The drawback of stepped sine is that it is slow compared to transient and random methods. At each step, time is required before the response attains steady state condition. It is the preferred method in literature when treating nonlinear behavior.

- **I**mpact excitation:
  *I*mpact excitation, with hammer testing is the standard for measuring linear FRFs in industry. Because of the easiness of applying the test *i*n situ and the broad frequency content in the impulse excites a high number of modes.

  For nonlinear testing, the method is not well suited. The energy of each individual frequency is small, making it hard to excite structural nonlinearities.

- **r**andom excitation:
  FRFs obtained by band limited *r*andom excitation will often appears linearized due to the randomness of the amplitude and phase of the excitation signal.

  Lidt forklaring af det! As for the impact excitation, the energy of each frequency is low, making it hard to drive structures into their nonlinear regime.

- **p**seudo-random:
  pseudo-random signal is a sum of multiple sine waves, with constant amplitude and the phase randomly selected from a uniform distribution between 180°C and −180°C

$$u(t) = \sum_{k=1}^{N_s} A_K \cos\left(2\pi k f_0 + \phi_k\right) \tag{4.1.1}$$

  where N_k is the number of sine components, A_k and ϕ_k is the amplitude and random phase of sine component k and f_0 is the fundamental frequency. Time series of pseudo random signal is obtained by applying the inverse DFT to the generated frequency domain representation of the signal.

  To avoid transient effects delay blocks are used, ie. acquisition only starts after repeating the same excitation block a number of times.

  The FRF is not distorted by leakage or windowing and due to the continuous excitation, the signal has a high SNR.

If FRF inspection is used for detection, only the stepped size excitation can be used of the mentioned types.**But how about pseudo random**

4.2 Signal treatment

Differentiation

Differentiation is hard without obtaining noisy results. Standard use of difference formulas, like the five-point central difference here, will result in noisy signals

$$y_i = \frac{1}{12\Delta t}\left(-y_{i+2} + 8y_{i+1} - 8y_{i-1} + y_{i-2}\right) \tag{4.2.1}$$

Chapter 5

Implementation

The methods presented in the previous chapters are implemented as a library in python and available from [22]. The code depends on the standard python libraries numpy, scipy and matplotlib and can run on all operating systems. Care have been taking in order to ensure correctness of the implementations; as much as it is possible examples from papers and data given from Liege have been recalculated to ensure that the same results were obtained. All code is written for this thesis and implement most notably:

- FEM code: generate FE matrices $\boldsymbol{M}, \boldsymbol{C}, \boldsymbol{K}$ from a *gmsh*-mesh file. Different types of elements are available. Boundary conditions are enforced on system matrices.
- Nonlinear newmark integration
- Morlet wavelet
- Restoring force surface
- Integration, filtering and periodicity calculation of signals
- NNM continuation and stability
- HB continuation, stability and bifurcation
- FNSI, linear and nonlinear parameter estimation. Stabilisation diagram for determining model order
- FRF calculation from periodic signals with multiple periods or from nonperiodic signals using spectral densities. Standard deviation of FRF between periods is calculated.
- Modal properties including MAC calculation.
- Sine sweep(linear and logarithmic) and random periodic excitation.
- Polynomial and piecewise cubic splines available for identification.
- Additional types of nonlinearities available for simulation with Newmark, HB and NNM: Piecewise linear and hyperbolic tangent(tanh), the latter only for damping.

As an example of the library approach, the following two examples shows how FNSI identification and HB continuation are done. Most methods returns a class storing all information, making multiple runs with different settings easy. To keep the examples short, they are run with default settings.

```
from numpy import np
from vib.signal import Signal
from vib.fnsi import FNSI
from vib.nlforce import NL_force, NL_polynomial
from vib.common import modal_properties

# load time signal
# nsper is the number of signals per period, iu the dof(s) where the force(s) works
mat = np.load(filename + '.npz')
u, ydd, fs, nsper, iu = mat['u'], mat['ydd'], mat['fs'], mat['nsper'], mat['iu']

# create class, integrate and select period(s) (fnsi works on displacements)
signal = Signal(u, fs, ddy=ddy)
signal.get_displ(lowcut, highcut)
signal.cut(nsper, per=[7,8])

# setup nonlinear type and where it works (-1: attached to ground)
inl = np.array([[0,-1], [1,-1]])
enl = np.array([3,3])
nl_pol = NL_polynomial(inl, enl)
nl = NL_force().add(nl_pol)
fmin, fmax = 0, 10
ims, nmodel = 22, 4
fnsi = FNSI(signal, nl, fmin, fmax)
fnsi.calc_EY()
fnsi.svd_comp(ims)
fnsi.id(nmodel)
# Get identified nl parameters and linear frf.
knl, H, He = fnsi.nl_coeff(iu)
# get linear modal parameters
modal = modal_properties(fnsi.A, fnsi.C)
# Done.
```

and for HB:

```
import numpy as np
from vib.hb.hb import HB
from vib.hb.hbcommon import hb_signal
from vib.nlforce import NL_force, NL_polynomial

# setup system
M = np.array([[m1,0],[0,m2]])
C = np.array([[c1,0],[0,c2]])
K = np.array([[k1+k2, -k2],[-k2, k2+k3]])
inl = np.array([[0,-1], [1,-1]])
enl = np.array([3,3])
knl = np.array([mu1, mu2])
nl_pol = NL_polynomial(inl, enl, knl)
nl = NL_force()
nl.add(nl_pol)
# starting frequency, force amplitude and force dof
f0, famp, fdof = 1, 3, 0

# create HB class, periodic solution and continuation incl stability and
# bifurcation.
hb = HB(M,C,K,nl)
omega, z, stab, lamb = hb.periodic(f0, famp, fdof)
hb.continuation()

# Run for another forcing level
hb2 = HB(M,C,K,nl)
hb2.periodic(f0, 2*famp, fdof)
hb2.continuation(bifurcation=False)
# Done
```

All the examples from the previous chapters are included in the examples directory, and should run on any python3 installation.

Chapter 6

Application

This chapter present two more involved cases of identification. The first case is identification of the COST beam, introduced as a standard test case for polynomial nonlinearities, ie. two polynomial nonlinearities at the same DOF. The second case demonstrate the usage of cubic spines to identify a system with two different clearances. The clearance distances are also found.

6.1 COST beam

The European action COST F3 nonlinear beam [12] was introduced in 2003 as a benchmark system for nonlinear vibrations. The experimental setup is shown in fig. **??** and consists of a clamped beam with a thin beam part at the end of the main beam.

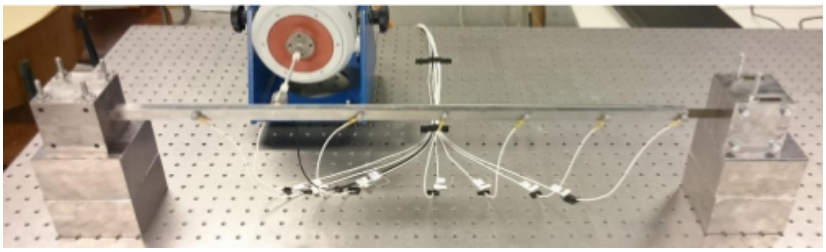

Figure 6.1.1: *Experimental setup for the COST beam. The setup is vertical to avoid gravitational effects which cannot be ignored due to the thin beam.*

Accelerations are measured evenly along the beam at seven locations and excited at node two. From Lenaerts, Kerschen, and Golinval [18] is it known that the system exhibit a (geometric) cubic nonlinearity due to large deformations of the thin beam and quadratic nonlinearity due to the clamped connection, both located at the tip of the main beam. Using data given at the Nolinsys course, the beam will be identified as an example of a MIMO system. After successful identification a FE model is built using the identified parameters, and used for further examination.

Identification

The time series were obtained by Nolinsys. The beam is excited with a periodic broadband input with flat amplitude spectrum, i.e. a multisine at low and high level.

At low and high level, the beam behaves linear and nonlinear respectively. To avoid leakage in the identification due to transient behavior, the periods used are selected from a plot of the periodicity. From fig. **??** is seen that transients are apparent in the first two periods and not apparent in periods 4-7, which are used for the identification.

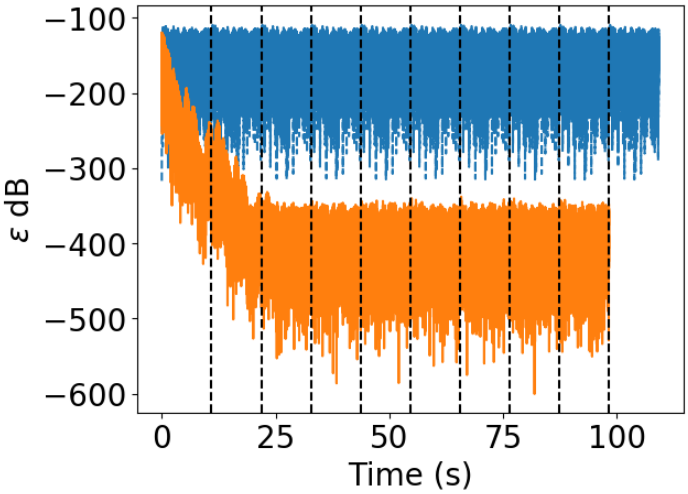

Figure 6.1.2: *Periodicity of recorded signal at high level wrt. the last period. Measured at the nonlinear dof.*

Figure **??** shows the stabilisation diagram used for determine model order. Fig. **??**(a) is used for linear identification and is fully stabilised at order 6. Fig. **??**(b) shows the nonlinear system identified with linear analysis, ie. without specifying nonlinear basis functions. The first mode does not stabilise, which normally indicates that the supplied basis functions are inadequate to represent the nonlinearity. Fig. **??**(c) shows the stabilisation after supplying a quadratic and cubic basis function. The first mode stabilises at model order 6, ie. the identification is most likely trustworthy and the nonlinearity are described by these functions.

The identified linear parameters are shown in table **??**. As expected, the first mode shows a hardening which is seen by the linear identification at high level. The linear parameters are estimated correctly at high level using the two basis functions.

Mode	Frequency (Hz)	Damping ration (%)	Deviation from linear freq. (%)
1	31.3	1.27	
2	143.6	0.29	
3	397.8	0.14	
1	33.1	1.08	5.7
2	144.1	0.29	0.3
3	398.0	0.14	0.05
1	31.3	1.27	10^{-3}
2	143.6	0.29	10^{-5}
3	397.8	0.14	10^{-6}

Table 6.1.1: *Estimated linear natural frequencies and damping ratios for the COST beam.* ***(upper)****: Low level, linear identification;* ***(middle)****: High level, linear identification;* ***(lower)****: High level, nonlinear identification.*

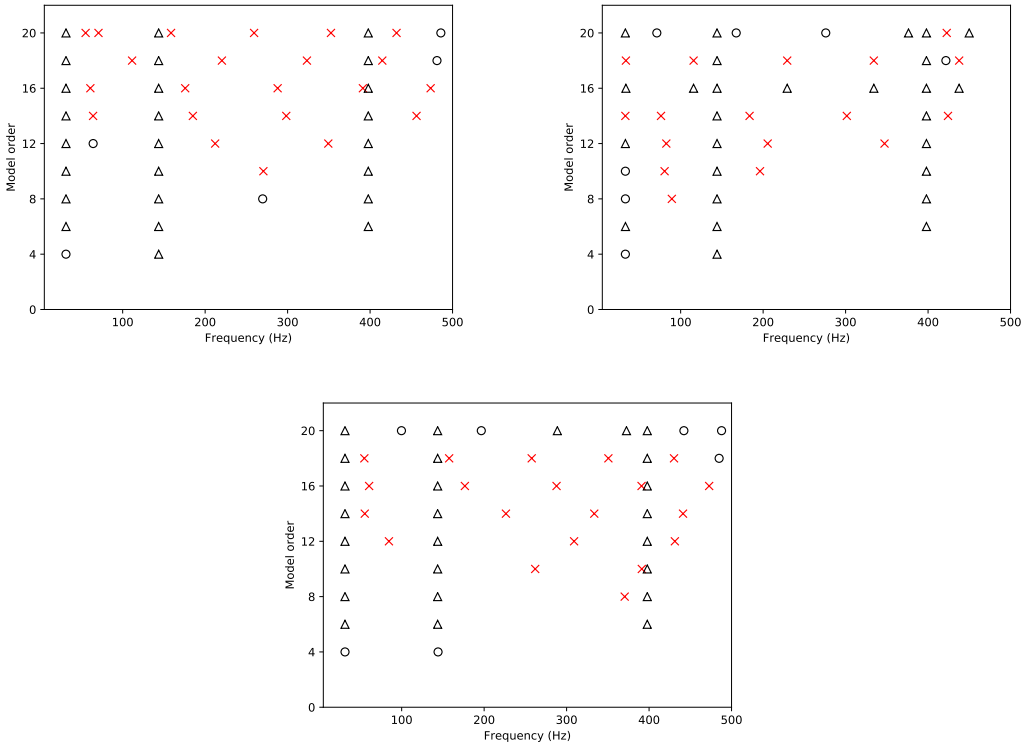

Figure 6.1.3: *Estimation of model order.* ×*(red): new pole;* ⋆*: stabilisation in natural frequency;* □*: extra stabilisation in damping ratio;* ∘*: extra stabilisation in MACX;* △*: full stabilisation. Stabilisation thresholds in natural frequency, damping ratio and MACX value are* $0.5\%, 2\%, 0.98$*, respectively. Not all types of stabilisation are present here.* ***(a)****: Low level, linear identification;* ***(b)****: High level, linear identification - no stabilisation of first mode;* ***(c)****: High level, nonlinear identification - stabilisation of first mode;*

The identified nonlinear coefficients are shown in figure **??**. The deviation of the real part is just within 1% and the imaginary part are around three orders of magnitude smaller, indicating a good identification.

Finally fig. **??** shows the FRF. Nonlinear distortion is seen from the signal at high level excitation. The FRF(blue) from low level excitation and identified by FNSI with basis functions(green) match.

Design

The test setup is modelled as shown in fig **??**, using 14 and 3 two-dimensional Bernoulli-Euler beam elements for the main and thin beam respectively. The connection between the two beams is modelled by an additional linear rotational stiffness, as suggested in [18], resulting in a model with 35 dofs.

The geometric properties are also given in [18] and listed together with the mechanical properties in tables **??**.

	Length(m)	Width (m)	Thickness (m)
Main beam	0.7	0.014	0.014
Thin beam	0.04	0.014	0.0005

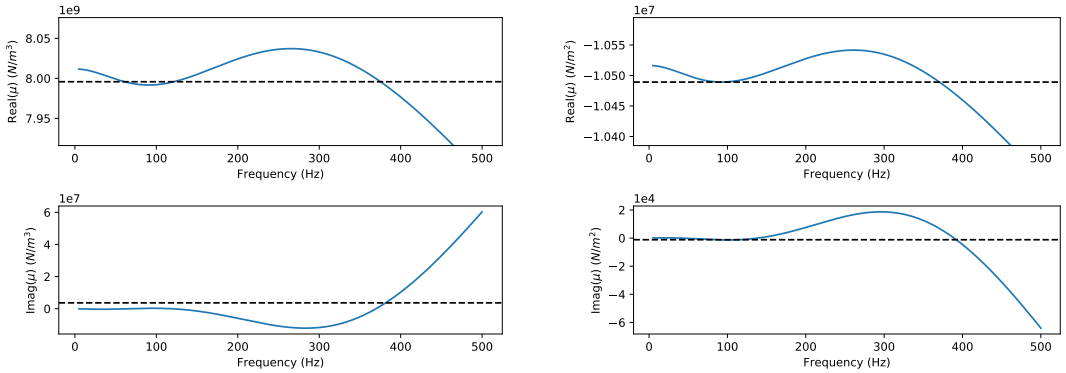

(a) **(b)**

Figure 6.1.4: *Real and imaginary part of estimated nonlinear coefficients μ_1 and μ_2. The variation of Re(μ) is seen to be within a 1 interval. The imaginary part is about three orders of magnitude smaller. Both indicates a good quality of the estimation. The spectral averages of the real part and ratio $log_{10}\frac{\mathrm{Re}(\mu)}{\mathrm{Im}(\mu)}$ are:* ***(a)****: $\mu_1 = 8.0 \times 10^9 m/n^3$, ratio = 3.34;* ***(b)****: $\mu_2 = -1.05 \times 10^7 m/n^2$, ratio = 3.96.*

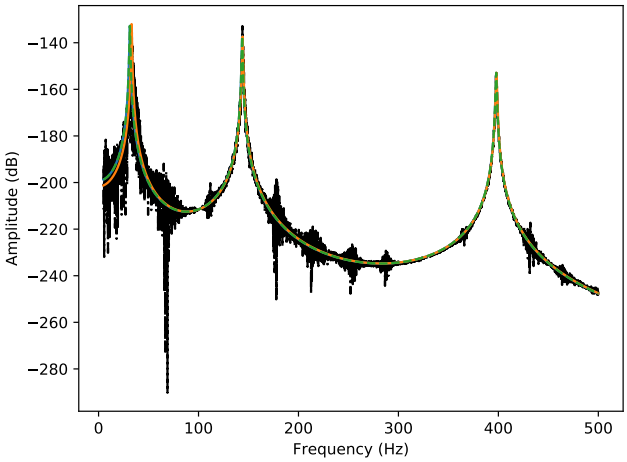

Figure 6.1.5: *FRF. Nonparametric(NP) is FRF directly from signal, parametric is identified FRF. ——: NP from high level excitation; ——: NP from low level excitation. ——: Linear parametric from high level excitation. - - - -: nonlinear parametric from high level excitation.*

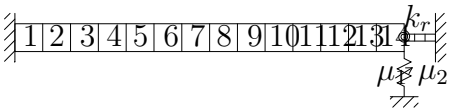

Figure 6.1.6: *FE model of the COST beam. Notice that it is depicted as a 2d FE model, but*

Young's modulus (N/m^2)	Density (kg/m^3)	μ_1 (N/m^3)	μ_2 (N/m^2)	Damping
2.05×10^{11}	7800	8×10^9	-1.05×10^7	$\boldsymbol{C} = 3 \times 10^{-7}\boldsymbol{K} + 5\boldsymbol{M}$

Table 6.1.2: *Geometric and mechanical properties for the nonlinear beam*

The damping is proportional damping and probably overestimated, giving a modal damping ration of 1.27% for the first linear mode which is high for a steel beam. But large displacements tends to be higher damped, thus the damping is not expected to be same for the linear and nonlinear case.

Figure **??** shows a comparison between a linear forward and backward sine sweep with a sweep rate and the NFRC computed by HB. The response is asymmetric due to the presence of the quadratic nonlinearity. The jump down occurs because of the hardening behavior.

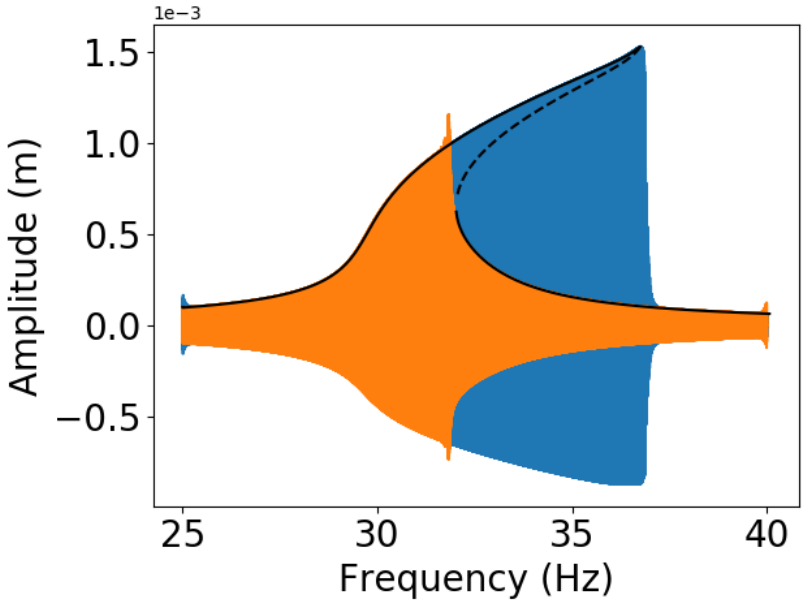

Figure 6.1.7: *Comparison between forward and backward sine sweep with HB. Sweep parameters: Amplitude: 3N, sweep rate: 10Hz/min. Stability is indicated for HB.*

Figure **??** shows the evolution of the harmonic components along the curve. As expected from the asymmetry, there is strong participation of the constant term, followed by the 2nd harmonic. Both due to the squared nonlinearity.

NNM mangler - Plot fra 1.nnm er beskrevet. 2.nnm mangler at blive beregnet. The NNMs of the underlying conservative system is shown in figure. The NNM frequency increases strongly with increasing energy, which is due to the hardening behavior of the cubic stiffness. The FEPs shows two branches emerging from the NNM backbone. These are called tongues and are said to reveal internal resonance. The tongue shows a 9:1 internal resonance between the first and third NNMs.

6.2 System with clearences

Ideen er at identificere clearence og parametre. Data genereres med en trilineær model. Men da Newmark, mv. kræver at stivheden er differentiabel, bruges et reguliseret udtryk. Det bliver forhåbent meget kortere end sidste eksempel. **Alt Mangler**.

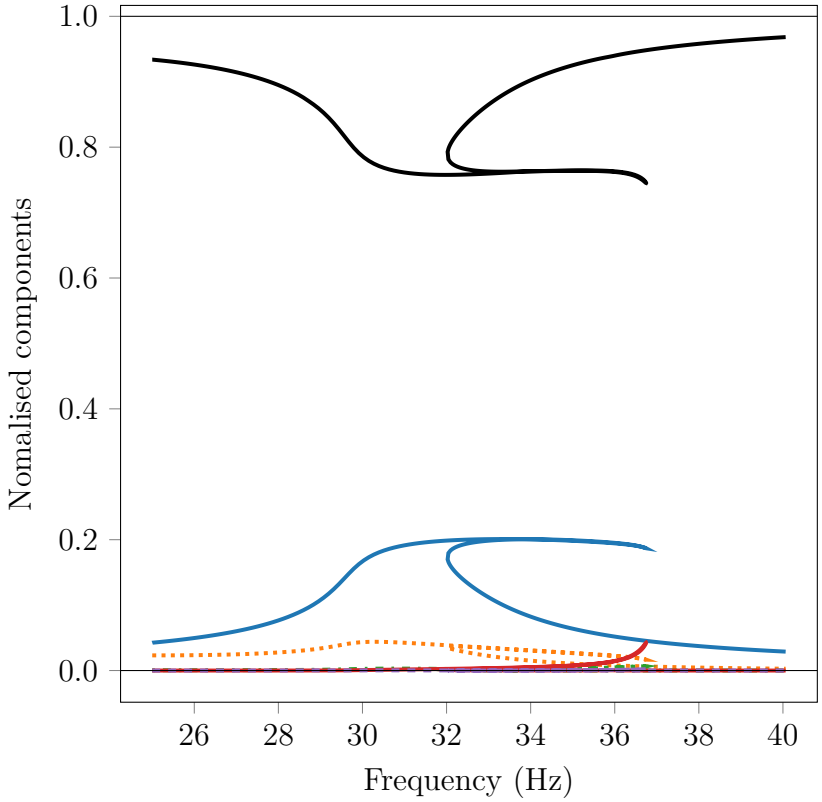

Figure 6.1.8: *Evolution of HB components.* ——: *Constant;* ——: *1st;* ·····: *2nd;* – – –: *3th;* ——: *4th;* - - - -: *5th;*

A trilinear model for stiffness' k_-, k, k_+ and clearances a_-, a_+ is given by,

$$f_{nl}(x) = \begin{cases} \text{sign}(x)\,(ka_+ + k_+(x - a_+)) & x \geq a_+ + \Delta_+ \\ p_+(t(x)) & a_+ + \Delta_+ > x > a_+ - \Delta_+ \\ kx & a_+ - \Delta_+ \geq -(a_- - \Delta_-) \\ p_-(t(x)) & -(a_- + \Delta_-) > x > -(a_- + \Delta_-) \\ \text{sign}(x)\,(ka_- + k_-(x - a_-)) & x \leq -(a_- + \Delta_-) \end{cases} \tag{6.2.1}$$

where x is the relative distance between the two DOFs defining the nonlinear connections. $2\Delta_\pm$ is the size of a regularization interval, used to enforce continuity of the first derivative.

The Hermite polynomials $p_\pm$ are defined as

$$p_\pm(t) = h_{00}(t)p_k + h_{10}(t)(x_{k+1} - x_k)m_k + h_{01}(t)p_{k+1} + h_{11}(t)(x_{k+1} - x_k)m_{k+1} \tag{6.2.2}$$

where p_k and p_{k+1} are the values of the restoring force at points $x_k = \text{sign}(x)(a - \Delta)$ and $x_{k+1} = \text{sign}(x)(a + \Delta)$, respectively. m_k and m_{k+1} are the values of the restoring force derivative at the same x_k and x_{k+1} points; they correspond to the stiffness coefficients k and $k_\pm$, respectively. The local scaled abscissa and h_{ij} functions are

$$
\begin{aligned}
t(x) &= \frac{x - x_k}{x_{k+1} - x_k} \\
h_{00}(t) &= 2t^3 - 3t^2 + 1 \\
h_{10}(t) &= t^3 - 2t^2 + t \\
h_{01} &= -2t^3 + 3t^2 \\
h_{11} &= t^3 - t^2
\end{aligned}
\tag{6.2.3}
$$

Figure **??** shows an example of a regulized nonlinear restoring force.

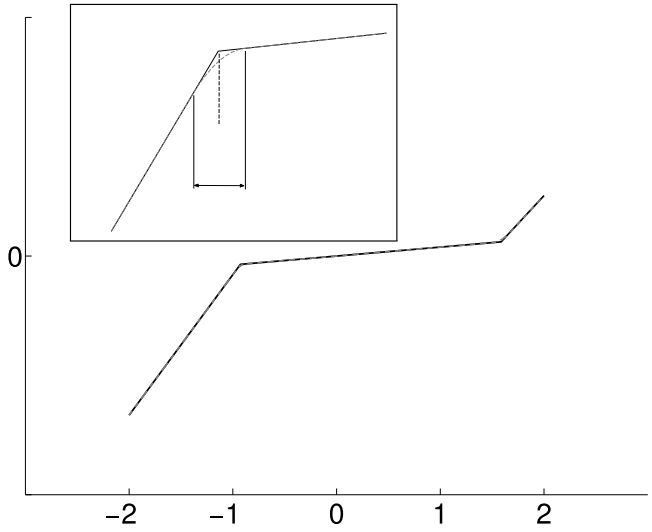

Figure 6.2.1: *Example of piecewise-linear restoring force. The insert image shows a closeup of the effect of the regularization* Δ.

Chapter 7

Conclusion

The focus of this report have been two-part. In the first part, methods for vibration-based identification of nonlinearities have been explored and validated. No assumption of the type of nonlinearity have been made, thus the models works equally well for boundary, geometric, etc. types of nonlinearities. Only stiffness have been treated; in theory the methods works just as well for damping, but in practice damping is much harder due to the much smaller magnitude and successful identification is still hard to obtain **Put ref på.**. Another subject that not have been treated, is identification with noisy signals. To get good estimates from noisy signals is difficult and more research have to be done in order to get consistent results.

In the second part, methods for investigating the behaviour of identified nonlinear systems are treated. On the successful identification in part one, a model is built and used for determine stability, bifurcations and internal resonances. Where the methods in the first part requires some understanding and knowledge about nonlinear system in order to obtain a good identification, the methods here are easier to use and do not require as much knowledge (that said, implementation wise they cannot be said to be easier).

One substantial lack in connecting the two parts, is the need to create a model after identification is done. Current research are focused on eliminating this step, and use the state space system identified by FNSI directly by the numerical methods of the second part. Numerically this is easy when both the FNSI and HB methods are implemented, but as shown in section **??** the FNSI method introduce spurious numerical artefacts, and as long as these artefacts are present, the state space formulation should not be used directly. Preventing artefacts in the FNSI method will be a big step forward in the seamless integration of the two methodologies.**Put ref på.**

References

[1] Randall J Allemang. "The modal assurance criterion–twenty years of use and abuse". In: *Sound and vibration* 37.8 (2003), pp. 14–23.

[2] RR Craig and MCC Bampton. "Coupling of substructures for dynamic analyses". eng. In: *Aiaa Journal* 6.7 (1968), pp. 1313–&. ISSN: 1533385x, 00011452. DOI: 10.2514/3.4741.

[3] Thibaut Detroux. "Performace and robustness of nonlinear systems using bifurcation analysis". PhD thesis. Aerospace and Mechanical Engineering Department, Mar. 2016.

[4] Thibaut Detroux, Ludovic Renson, and Gaëtan Kerschen. "The Harmonic Balance Method for Advanced Analysis and Design of Nonlinear Mechanical Systems". eng. In: *springer* (2016). DOI: 10.1.1.839.5497.

[5] T. Detroux et al. "The harmonic balance method for bifurcation analysis of large-scale nonlinear mechanical systems". eng. In: *Computer Methods in Applied Mechanics and Engineering* 296 (2015), pp. 18–38. ISSN: 18792138, 00457825. DOI: 10.1016/j.cma.2015.07.017.

[6] A. Dhooge, W. Govaerts, and Yu. A. Kuznetsov. "MATCONT: A MATLAB Package for Numerical Bifurcation Analysis of ODEs". In: *ACM Trans. Math. Softw.* 29.2 (June 2003), pp. 141–164. ISSN: 0098-3500. DOI: 10.1145/779359.779362.

[7] Scott W Doebling et al. *Damage identification and health monitoring of structural and mechanical systems from changes in their vibration characteristics: a literature review*. Tech. rep. Los Alamos National Lab., NM (United States), 1996. DOI: http://dx.doi.org/10.2172/249299.

[8] T. Dossogne et al. "Nonlinear ground vibration identification of an F-16 aircraft - Part II: Understanding nonlinear behaviour in aerospace structures using sine-sweep testing". eng. In: *International Forum on Aeroelasticity and Structural Dynamics, Ifasd 2015* (2015).

[9] D.J. Ewins. *Modal testing: Theory, Practice and Application*. eng. Research Studies Press, 2000, 562 s.

[10] M.I. Friswell and J.E. Mottershead. *Finite element model updating in structural dynamics*. eng. Vol. 38. Kluwer, 1995, 286 s. ISBN: 0792334310.

[11] M Gatto, B Peeters, and G Coppotelli. "Flexible shaker excitation signals for improved FRF estimation and non-linearity assessment". In: *Proceedings of the ISMA 2010 International Conference on Noise and Vibration Engineering*. 2010.

[12] J.-C. GOLINVAL and M. LINK. "COST Action F3 'Structural Dynamics' (1997–2001)—An European Co-Operation In The Field Of Science And Technology". In: *Mechanical Systems and Signal Processing* 17.1 (2003), pp. 3–7. ISSN: 0888-3270. DOI: http://dx.doi.org/10.1006/mssp.2002.1533.

[13] Michael Blom Hermansen. "Vibration-based identification of beam boundary models". MA thesis. Technical university of Denmark, 2017.

[14] Jon Juel Thomsen. *Vibrations and stability : advanced theory, analysis, and tools*. Springer, 2003, 404 s. ISBN: 9783540401407.

[15] G. Kerschen et al. "Nonlinear normal modes, Part I: A useful framework for the structural dynamicist". eng. In: *Mechanical Systems and Signal Processing* 23.1 (2009), pp. 170–194. ISSN: 10961216, 08883270. DOI: 10.1016/j.ymssp.2008.04.002.

[16] G Kerschen et al. "Past, present and future of nonlinear system identification in structural dynamics". eng. In: *Mechanical Systems and Signal Processing* 20.3 (2006), pp. 505–592. ISSN: 10961216, 08883270. DOI: 10.1016/j.ymssp.2005.04.008.

[17] Knud Abildgaard Kragh. "Detection, Localization, and Characterization of Structural Nonlinearities from Dynamic Measurements". MA thesis. DTU Mechanical Engineering, 2010.

[18] V Lenaerts, G Kerschen, and JC Golinval. "Identification of a continuous structure with a geometrical non-linearity. Part II: Proper orthogonal decomposition". eng. In: *Journal of Sound and Vibration* 262.4 (2003), pp. 907–919. ISSN: 10958568, 0022460x. DOI: 10.1016/S0022-460X(02)01132-X.

[19] S. Marchesiello and L. Garibaldi. "A time domain approach for identifying nonlinear vibrating structures by subspace methods". eng. In: *Mechanical Systems and Signal Processing* 22.1 (2008), pp. 81–101. ISSN: 10961216, 08883270. DOI: 10.1016/j.ymssp.2007.04.002.

[20] S. F. Masri and T. K. Caughey. "A nonparametric identification technique for nonlinear dynamic problems". eng. In: *Transactions of the Asme. Journal of Applied Mechanics* 46.2 (1979), pp. 433–47, 433–447. ISSN: 15289036, 00218936. DOI: 10.1115/1.3424568.

[21] SF Masri et al. "Identification of the state equation in complex non-linear systems". eng. In: *International Journal of Non-linear Mechanics* 39.7 (2004), pp. 1111–1127. ISSN: 18785638, 00207462. DOI: 10.1016/S0020-7462(03)00109-4.

[22] Paw Møller. *Vibration code, python*. Oct. 2017. URL: https://github.com/pawsen/vib.

[23] Ali H Nayfeh and Balakumar Balachandran. *Applied nonlinear dynamics: analytical, computational and experimental methods*. John Wiley & Sons, 2008.

[24] J. P. Noel and G. Kerschen. "Frequency-domain subspace identification for nonlinear mechanical systems". eng. In: *Mechanical Systems and Signal Processing* 40.2 (2013), pp. 701–717. ISSN: 10961216, 08883270. DOI: 10.1016/j.ymssp.2013.06.034.

[25] J. P. Noël and G. Kerschen. "Nonlinear system identification in structural dynamics: 10 more years of progress". eng. In: *Mechanical Systems and Signal Processing* 83 (2016), pp. 2–35. ISSN: 10961216, 08883270. DOI: 10.1016/j.ymssp.2016.07.020.

[26] Jean-Philippe Noël. "A Frequency-Domain Approach to Subspace Identification of Nonlinear Systems - Application to Aerospace Structures". PhD thesis. Aerospace and Mechanical Engineering Department, Feb. 2014.

[27] M. Peeters et al. "Nonlinear normal modes, Part II: Toward a practical computation using numerical continuation techniques". eng. In: *Mechanical Systems and Signal Processing* 23.1 (2009), pp. 195–216. ISSN: 10961216, 08883270. DOI: 10.1016/j.ymssp.2008.04.003.

[28] L. Renson, G. Kerschen, and B. Cochelin. "Numerical computation of nonlinear normal modes in mechanical engineering". eng. In: *Journal of Sound and Vibration* 364 (2016), pp. 177–206. ISSN: 10958568, 0022460x. DOI: 10.1016/j.jsv.2015.09.033.

[29] Ludovic Renson. "Nonlinear Modal Analysis of Conservative and Nonconservative Aerospace Structures". PhD thesis. Aerospace and Mechanical Engineering Department, Universitet de Liege(ULG), Feb. 2014.

[30] Rosenberg. "On nonlinear vibrations of systems with many degrees of freedom". und. In: *Advances in Applied Mechanics* (1966), pp. 155–242, 155–242.

[31] S. W. Shaw and C. Pierre. "Normal modes for non-linear vibratory systems". eng. In: *Journal of Sound and Vibration* 164.1 (1993), pp. 85–124, 85–124. ISSN: 10958568, 0022460x. DOI: 10.1006/jsvi.1993.1198.

[32] A. F. Vakakis and R. H. Rand. "Normal modes and global dynamics of a two-degree-of-freedom non-linear system. I. Low energies". eng. In: *International Journal of Non-linear Mechanics* 27.5 (1992), pp. 861–74, 861–874. ISSN: 18785638, 00207462. DOI: 10.1016/0020-7462(92)90040-E.

[33] Alexander F Vakakis et al. *Nonlinear targeted energy transfer in mechanical and structural systems*. eng. Vol. 156. Springer Science & Business Media, 2008, pp. 1–1033. ISBN: 9781402091254. DOI: http://dx.doi.org/10.1007/978-1-4020-9130-8.

[34] K. Worden. "Data processing and experiment design for the restoring force surface method, part I: integration and differentiation of measured time data". eng. In: *Mechanical Systems and Signal Processing* 4.4 (1990), pp. 295–319. ISSN: 10961216, 08883270. DOI: 10.1016/0888-3270(90)90010-I.

[35] Keith Worden and Geoffrey R Tomlinson. *Nonlinearity in structural dynamics: detection, identification and modelling*. CRC Press, 2000.